PCCP

Oxidative Decomposition of Dimethyl Methylphosphonate on rutile TiO2(110): the role of oxygen vacancies

Journal:	*Physical Chemistry Chemical Physics*
Manuscript ID	CP-ART-05-2022-002246.R1
Article Type:	Paper
Date Submitted by the Author:	24-Aug-2022
Complete List of Authors:	Tesvara, Celine; University of California Los Angeles, Chemical Engineering Walenta, Constantin; Harvard University, Chemistry and Chemical Biology Sautet, Philippe; University of California Los Angeles,

Oxidative Decomposition of Dimethyl Methylphosphonate on rutile TiO_2(110): the role of oxygen vacancies

Celine Tesvara[a], Constantin Walenta[b], Philippe Sautet[a,c*]

[a] Chemical and Biomolecular Engineering Department, University of California, Los Angeles, Los Angeles, CA 90095, USA

[b] Department of Chemistry & Chemical Biology, Harvard University, Cambridge, MA 02138, USA

[c] Chemistry and Biochemistry Department, University of California, Los Angeles, Los Angeles, CA 90095, USA

Corresponding Author: sautet@ucla.edu

Abstract

The decomposition of dimethyl methylphosphonate (DMMP, $(CH_3O)_2P(O)(CH_3)$), a simulant to the toxic nerve agent Sarin, on the rutile TiO_2(110) surface has been studied with temperature programmed desorption (TPD) and density functional theory (DFT) calculations. The reactivity of the TiO_2(110) surface for DMMP decomposition is shown to be low, with mainly molecular desorption and only a small fraction of methanol and formaldehyde decomposition products seen from TPD at around 650K. In addition, this amount of products is similar to the number of O vacancies on the surface. DFT calculations show that O vacancies are key for P-OCH_3 bond cleavage of DMMP,

lowering the barrier by 0.7 eV, and enabling that reactive process to occur at around 600K. This is explained by the closer position of DMMP with respect to the surface in the presence of the O vacancy. Calculations show that the produced methoxy groups can transform to gas phase formaldehyde and methanol at the considered temperature (600K), in agreement with experiments. O-C bond cleavage of DMMP is also a viable pathway at such high temperature (600K) for DMMP decomposition on r-TiO_2, even in the absence of O vacancies, but the formation of gas phase product is energetically unfavorable. O vacancies hence are the active site for decomposition of DMMP into gas phase products on r-TiO_2(110).

Introduction

Sarin is a toxic compound that disrupts the nervous system, subsequently making it one of the most dangerous Chemical Warfare Agents (CWAs).[1–3] With a renewed interest in safe handling and decontamination of toxic CWAs, there is a critical need for improved protective equipment capable of rendering these chemicals harmless under ambient conditions. Understanding the elementary steps in which these organophosphonates can be catalytically decomposed is an important knowledge for the design of such equipment.

Due to the extreme toxicity of CWA, experimental studies often substitute the nerve agents studied with non-hazardous compounds exhibiting similar structural geometry and functional groups. Particularly dimethylmethylphosphonate (DMMP) is used as a simulant of Sarin. Sarin and DMMP both share the O=P(OR_1)(X)(R_2) structure, where R_1 and R_2 are alkyl groups and X an electronegative monovalent substituent. In the case of DMMP,

X is another alkoxy (OR_1 group) and R_1 and R_2 are methyl groups. In sarin, R_1 is isopropyl, R_2 methyl and X fluorine. DMMP is considered to provide a good initial estimation for Sarin's decomposition chemistry while being relatively non-toxic.

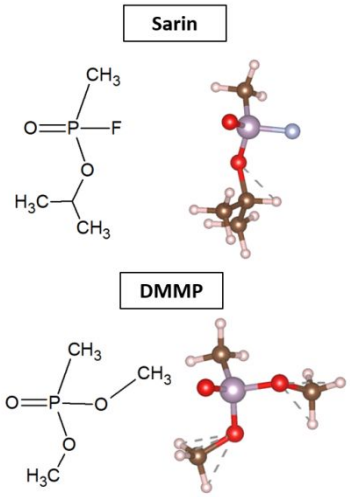

Figure 1: Chemical structures of Sarin (top) and DMMP (bottom) illustrating their similarity.

Metal oxides, including CuO[4,5], MoO_3[5,6], MoO_2[7], Al_2O_3[8–11], MgO[12–15], CeO_2[9,16], Fe_2O_3[17], Fe_3O_4[18], and TiO_2[19–22] are known to promote the decomposition of organophosphorus molecules at ambient temperature.[23] Studies using Fourier transform infrared spectroscopy (FTIR) and X-ray photoelectron spectroscopy (XPS) on metal oxides such as MoO_2, CeO_2, CuO, Al_2O_3, and TiO_2 indicated that DMMP adsorbs via the interaction between the oxygen of P=O group and surface metal cation.[4,7,16,24,25] Decomposition wise, one of the earliest works on metal oxides uses IR to follow DMMP decomposition on the oxides of Al, Mg, La and Fe. P-OCH_3 bond cleavage occurs for DMMP thermal decomposition on aluminum, magnesium and lanthanum oxide, whereas in the case of iron oxide, ceria, and cupric oxide, P-CH_3 bond activation was also observed.[4,24] Common thermal decomposition products include methanol, formaldehyde, carbon

dioxide, and carbon monoxide.[16,17,26–28] Dimethyl ether is also formed from DMMP decomposition on thin films of Fe_3O_4(111) and on MoO_3.[7,22,27,29]

On powdered titania, FTIR studies of DMMP decomposition show between 300 K and 400 K a decrease of stretching modes corresponding to methoxy groups in DMMP, with the increase of the band linked with surface methoxy species. This was interpreted as resulting from the cleavage of a P-OCH_3 bond in DMMP, transferring a methoxy onto surface Ti atoms and forming methyl methylphosphonate (MMP).[21,30] The formation of gas phase methanol was observed in the case of hydroxylated TiO_2 anatase.[19] Powdered TiO_2 do not activate the P-CH_3 bond until temperature above 800 K.[8,20,24,31,32]

Model studies on single crystal rutile TiO_2(110) under ultra-high vacuum conditions show that DMMP adsorption occurs via the dative bond between the P=O group and Ti_{5c}, and that molecular desorption is observed up to 550K, suggesting a rather low reactivity at room temperature.[26] Decomposition products consisting of methane, methyl and hydrogen evolve at 500 K while phosphorus containing species remains on the surface. The low reactivity and the observed decomposition products contrast with experiments using powder samples in ambient conditions. The observed reactivity on single crystal TiO_2 surfaces can be affected by the presence of various defects on TiO_2, mainly O vacancies, so that the understanding of the intrinsic reactivity of single crystal surfaces requires additional fundamental insights from surface science and modelling.

The fundamental knowledge about decomposition reaction pathways on various metal oxide surfaces used and our understanding of the influence of surface structure on the elementary steps of DMMP decomposition, both thermodynamically and kinetically, remains limited. Studies on metal organic frameworks such as zirconium(IV) based MOF

(as UiO-66) have shown that the surface hydroxyl groups are influential in DMMP interaction and dissociative adsorption,[29,33–36] whereas in the case of metal oxides DMMP may interact with the surface even in the absence of hydroxyl groups. On oxygen terminated MoO_3, oxygen vacancy have been shown to play a role in altering the surface Lewis acidity, and subsequently the reactivity for DMMP decomposition.[6] More generally, surface point defects on metal oxides such as oxygen vacancies, have been shown to have an important effect towards surface reactivity in reactions such as methanol dehydrogenation[37,38], H_2S dissociation[39], water dissociation[40], and hydrogen evolution[41] in particular for the case of rutile and anatase surfaces. All these studies hint at a possible important role held by surface defects on reactivity.

The rutile form of titanium oxide has been studied quite extensively and procedures for creating well-defined surfaces with specific types of defects, including bridging oxygen vacancies,[42–51] are established. Bridging oxygen vacancy defects are known to play a key role as active sites on rutile TiO_2 for various reactions such as chemisorption of hydrogen[52,53], chemisorption and oxidation of CO[52,54–56], dissociation of water[40,53,57–70], dissociation of O_2[71–74], photo-oxidation and decomposition of methanol[37,75–83], and formaldehyde oxidation[80,84–89]. A comprehensive review by Henderson on past literatures summarizes how H_2O dissociates at bridging oxygen vacancy sites to produce two hydroxyls on the surface, whereas on the pristine surface, the interaction between water and surface is weak.[64] In the case of methanol, recombinative desorption is facile and observed at 350 K. However, exposure to O_2 leads to oxygen adatoms near vacancy sites which significantly increases the O-H bond cleavage of methanol, creating surface methoxy species.[37] With the wide agreement over how bridging oxygen vacancy

increases reactivity of many small molecules, it is probable that these surface defect states can have an impact towards the decomposition of organophosphorus CWA as well.

In this work, several different channels for decomposition of DMMP are investigated on the pristine and defective r-TiO_2(110) surface using a combination of theory and experiment. We chose TiO_2(110) as this surface is stable and exhibit accessible Lewis acid sites and oxygen vacancy defects that may help the reactivity of DMMP decomposition.[45,47] We aim to provide insights on the preferred decomposition pathway of DMMP on r-TiO_2(110) and on how oxygen vacancies may affect the preferred decomposition steps. DFT was employed to study the adsorption geometries and energies and to explore possible decomposition mechanisms. Most crucially, DFT explains the possible decomposition channel shown by our TPD experiment.

Computational Methods

The density functional theory calculations were performed using the Vienna Ab Initio Simulation Package.[90,91] The Perdew-Burke-Ernzerhof (PBE) functional within the generalized gradient approximation (GGA) was employed to describe the exchange and correlation energy with addition of a dDsC dispersion correction to describe the van der Waals interactions.[92–94] The Projector Augmented Wave (PAW) method was used to describe the electron-ion interactions. The one-electron states were developed on a basis of plane waves with a kinetic energy cutoff of 500 eV.[95–97] Due to the onsite coulomb repulsion of the Ti 3d orbitals, the calculations included the effective Hubbard U (DFT+U) parameter of 4.2 eV on Ti following the Dudarev approach.[98,99] The U value 4.2 eV was taken as it correctly depicts the electronic structure features observed experimentally with TiO_2, particularly the localized nature of electrons on surfaces with oxygen vacancies.[48]

The electronic energies were converged within 10^{-6} eV threshold and the atomic force convergence criterion for geometry optimizations was set to 0.03 eV/atom. The transition states were calculated using the Nudged Elastic Band Method with 8 images. Due to the expensive computational demands of the NEB method, once a force limit of 0.1 eV is reached, the search of transition state is further continued with the Quasi Newton method until the forces converges under 0.03 eV/atom.

The adsorption energies are calculated with equation 1:

$$E_{ads} = E_{surf+DMMP} - E_{surface} - E_{DMMP(g)} \quad (1)$$

The approximate kinetic rate constant for each elementary step on the TiO_2 surface was calculated using the Transition State Theory approximation, with vibrational contribution to entropy neglected:

$$k = \left(\frac{k_b T}{h}\right) * \exp\left[\frac{-(E_{TS} - E_R)}{k_b * T}\right]$$

Where E_{TS} is the energy of the transition state and E_R is the energy of the reactant.

Computational Model

The periodic slab of rutile TiO_2 (110) was cut from the TiO_2 bulk structure optimized using the PBE+U functional. The calculated lattice constants for TiO_2 bulk are a = 4.68 Å and c = 3.03 Å, slightly longer (3 %) than experimental values of a = 4.54 Å and c = 2.94 Å, in agreement with previous studies.[54,100,101] The bulk calculations use a gamma centered k-points mesh of 4x4x4.

The TiO_2(110) surface is modelled as a 2x4 super cell with lattice vectors a = 13.16 Å and b = 12.07 Å (fig. 2). The surface cell contains four O-Ti-O trilayers (12 atomic layers) with a vacuum distance of 15 Å between slabs to avoid interaction. The geometry of the bottom most three atomic layers is frozen to the bulk structure. The surface presents 4 types of atoms based on their coordination, namely Ti_{5c}, Ti_{6c}, O_{2c}, and O_{3c}. These atoms form rows in the [001] direction. The top-most layer consists of O_{2c} rows (bridging oxygen row) and exposed Ti_{5c} rows sandwiched between two O_{3c} rows. Ti_{6c} rows reside beneath top-most O_{2c} bridging oxygen row. Among the two types of oxygen atoms, oxygen vacancy at bridging oxygen site was found to be more stable[49,102,103], and thus the defect sites considered are the vacancy on the O_{2c} bridging site only. In each supercell only one vacancy is created which corresponds to a 0.125 ML coverage to mimic experimentally

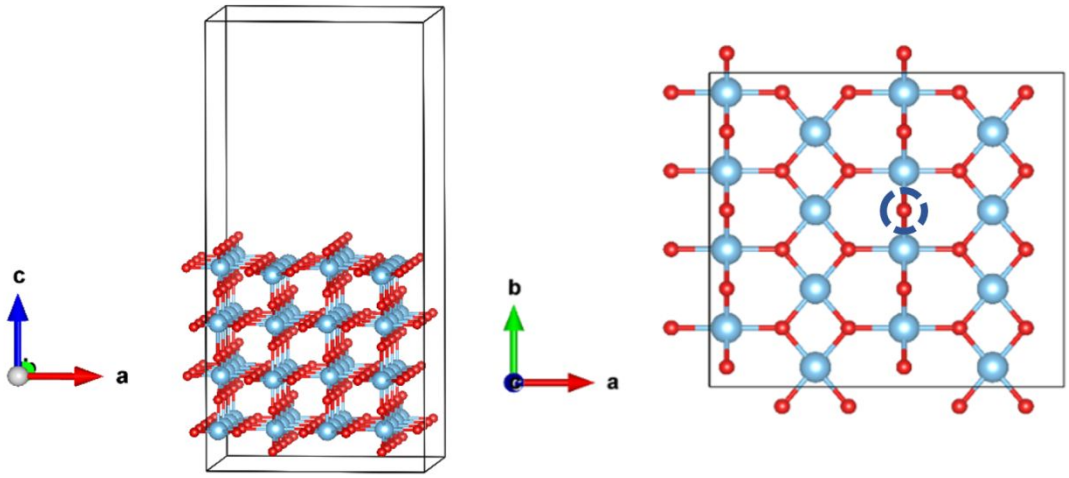

Figure 2: Rutile TiO_2(110) Surface Model. (Left) Side view of the pristine TiO_2 (110) supercell and (Right) Top view of defective TiO_2(110) supercell with an O_{2c} oxygen vacancy (indicated by a broken line circle, since a subsurface O atom is seen below at the same x, y position).

observed vacancy coverage (between 0.08 to 0.15 ML)[37,47,104]. Only the gamma point is use for surface calculations. Further test shows that using a k-points mesh of 3x3x1 gives no significant difference compared to gamma point calculations. Tests have also been

performed for adsorption energy, transition state energy and surface reaction energy with a larger 3x6 unit cell or a thicker model with 6 trilayers, and the largest difference was 0.05 eV, hence validating the model choice (see SI pages 1-2, Figure S1, table S1 and S2). A 2x3 unit cell was also considered for high coverage calculations.

The dipole-dipole interaction between each slab in the z direction was corrected using the Harris correction and Makov-Payne method as implemented in VASP.[105]

Experimental Methods

Desorption and reaction of DMMP is studied in an ultra-high vacuum apparatus described previously.[106,107] A clean TiO_2(110) surface with a bridge-bonding oxygen vacancy concentration of ≤2% of a monolayer (with respect to the Ti-surface sites) was obtained by cycles of Ar^+-sputtering and vacuum annealing 780 K.[106] DMMP (purity ≥97%, Sigma-Aldrich) was purified by pump freeze cycles. The TiO_2 crystal quality has been routinely checked by Auger Electron Spectroscopy and temperature programmed desorption of H_2O. The bridge-bonding oxygen vacancy concentration was determined to be 1.5% ±0.5% by water desorption (Fig. S2).

Before every experiment, the designated gas line system was flushed and pumped multiple times and further passivated with more than 1 h of DMMP exposure to avoid contamination by any hydrolysis products as determined by the vapor pressure in the gas line of 0.11 Torr.[108] DMMP exposures were performed with a pressure of 5×10^{-10} Torr for 60 s unless otherwise stated, which lead to a monolayer saturation coverage at a crystal temperature of 200 K. The exposure amounts do not correct for the enhancement in flux of the needle dozer, which was determined to be 27 previously in comparison to

Langmuir exposures. Temperature programmed desorption and reaction experiments were performed with the crystal positioned in a line-of-sight geometry with the quadrupole mass spectrometer and a constant heating rate of 1 K/s. The highest temperature is kept to 780 K to avoid unwanted reductions and reconstructions of the TiO_2(110) surface.[42,109] The masses monitored include m/e of 2, 15, 16, 18, 27, 28, 29, 30, 31, 32, 33, 35, 44, 46, 47, 79 and 124. The gas-phase products were identified by their fragmentation patterns and corrected fragmentation pattern contributions and mass spectrometer sensitivity. An additional trace to show the unambiguous identification of methanol and formaldehyde is shown in figure S3 in the supporting information. The quantitative reactivity analysis is done exactly as described in earlier work[83,110] with the ionization sensitivities of the molecules.[111–113]

Results

Temperature programmed studies of DMMP on r-TiO_2(110)

Molecular desorption of DMMP predominates on r-TiO_2(110), occurring over a broad temperature range, 200-500 K (fig. 3), in agreement with prior literature.[28] A small amount of methanol and formaldehyde, in similar ratio, is also produced at ~650 K, accounting for 2% of a monolayer. The amount of methanol can be quantified by a direct comparison of integrals with a monolayer saturation coverage from a pure methanol exposure control experiment.

The 2% of reacted products are in excellent agreement with the bridge-bonded oxygen vacancy concentration of ≤2%. No other reaction products are detected. The concomitant evolution of methanol and formaldehyde is consistent with disproportionation of adsorbed

methoxy.[37,77,79,114–118] These methoxy species must result from DMMP dissociation, in agreement with the further presented calculations. Based on the gaseous products, 14% of ML of DMMP molecules desorb from the surface, accounting for 87% of total gaseous products. Some of the DMMP reacts and is trapped on the surface as $PO_xC_yH_z$ species based on a small P and C signal a subsequent Auger Electron Spectrum (Fig. S4), in agreement with earlier work on TiO_2(110)[28,119,120].

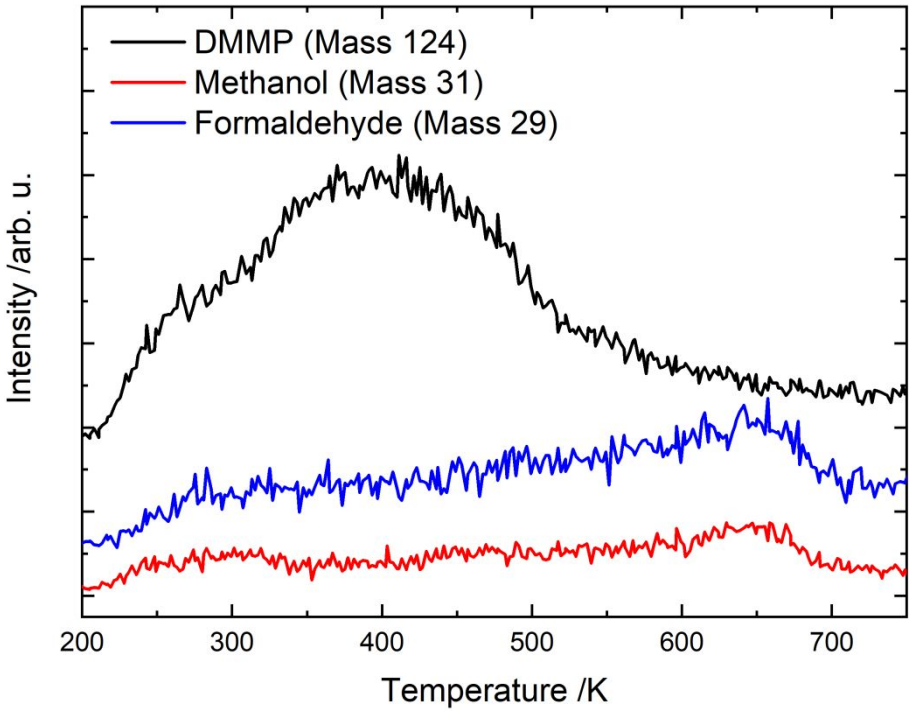

Figure 3: Temperature programmed desorption/reaction of DMMP on reduced TiO_2(110) shows that DMMP desorbs intact from the titania surface between 200 K and 500 K, while only minor amounts of methanol and formaldehyde are detected. No other reaction products were detected. Adsorption of DMMP was carried out at 200 K to avoid multilayer formation at 190 K.[108] The concomitant desorption of methanol and formaldehyde coincides with the temperature were methoxy disproportionation is observed on the TiO_2(110) surface.[114]

Molecular desorption of DMMP around room temperature from oxide surfaces has commonly been observed for reducible oxides including Ce[16] and Ti added with Cu, Au, Pt and Ni clusters. [28,119,120] In contrast, DMMP reacts at room temperature due to the presence of metal cation sites and additional oxygen adatoms on a thin film of

Fe_3O_4(111).[108] In agreement with studies on powdered materials,[20,21] thermal energy greater than that at room temperature is needed to form methyl methylphosphonate and adsorbed methoxy from DMMP.

DMMP adsorption and decomposition on the pristine r-TiO_2(110)

Two favorable geometries of molecular DMMP bound to the perfect r-TiO_2(110) surface were identified from our DFT calculations (Fig. 4). One DMMP molecule is adsorbed on the (2x4) r-TiO_2(110) unit cell, hence corresponding to a low coverage of 1/8 ML (1 molecule for 8 Ti_{5c} surface atom). Interaction between the oxo (O_I) atom and 5-coordinate Ti (Ti_{5c}) is most favorable, with an adsorption energy of -2.35 eV (-227 kJ/mol). This geometry (S1) is stabilized by an interaction between the oxygen on one methoxy (O_{II}) and a neighboring Ti_{5c} (fig. 4 left), with the methoxy tilting towards the surface. This geometry agrees well with past literatures.[68,121–125] The distance between O_I to its nearest Ti_{5c} is 2.11 Å (primary interaction) compared to a Ti-O_{II} distance of 2.42 Å (secondary interaction). This binding mode is called η_2, since two O atoms from the molecule interact with the surface. The other stable adsorption geometry with adsorption energy of -1.71 eV (-164 kJ/mol) involves only the O_I-Ti_{5c} interaction (fig. 4 right), hence called η_1 and is significantly less stable.

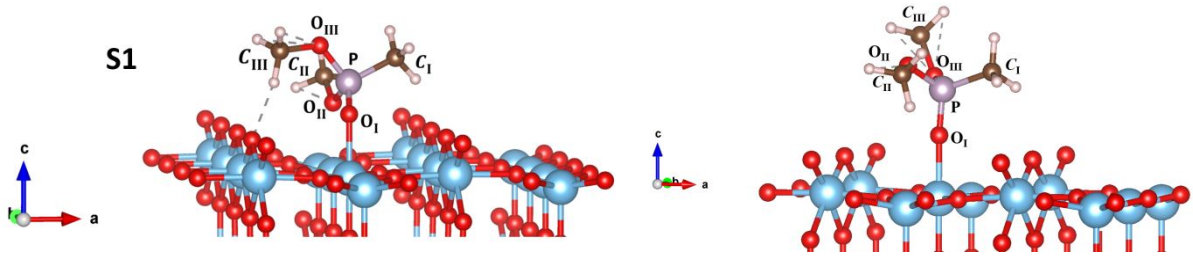

Figure 4: Molecular adsorption of DMMP on pristine r-TiO_2(110) at low coverage. Most stable adsorption mode (η_2, left) with adsorption energy of -2.35 eV and second most stable adsorption mode (η_1, right) with adsorption energy of -1.71 eV. Roman numerals subscripts have been used to distinguish the different oxygen and carbon atoms.

Since experiments show a saturation coverage at 200K, we also examined situations of high coverage, including lateral interactions. This was performed by adsorbing 2 to 4 molecules on the (2x4) or (2x3) surface unit cells, describing coverage values between 1/8 and 2/3 ML. Figure 5 shows the DMMP differential adsorption energy as a function of coverage. For each coverage, only one molecule is desorbed, and that molecule can be either a η_2 or a η_1 binding mode depending on the considered structure. If inequivalent molecules are present on the surface, the one presenting the weakest adsorption energy is removed, so that the most strongly bound adsorbates remain on the surface. Details on structures can be found in supporting information (see SI pages 7-10 and Fig. S5-S8). Figure 5 shows a marked decrease of the DMMP differential adsorption energy upon coverage increase, with a range of adsorption energies between -2.35 eV for the low coverage to -0.7 eV for 2/3 ML. The adsorption energies of the η_1 modes remain 0.64 to 0.39 eV less stable than that of the η_2 geometries. Beyond 0.5 ML coverage, the additional DMMP molecule can only weakly interact, with an adsorption energy of -0.7 eV, mainly by van der Waals and electrostatic interactions, the O(DMMP)…Ti distance being 3.99 Å. The range of weaker adsorption energy at high coverage is consistent with the measured distribution of desorption temperatures.

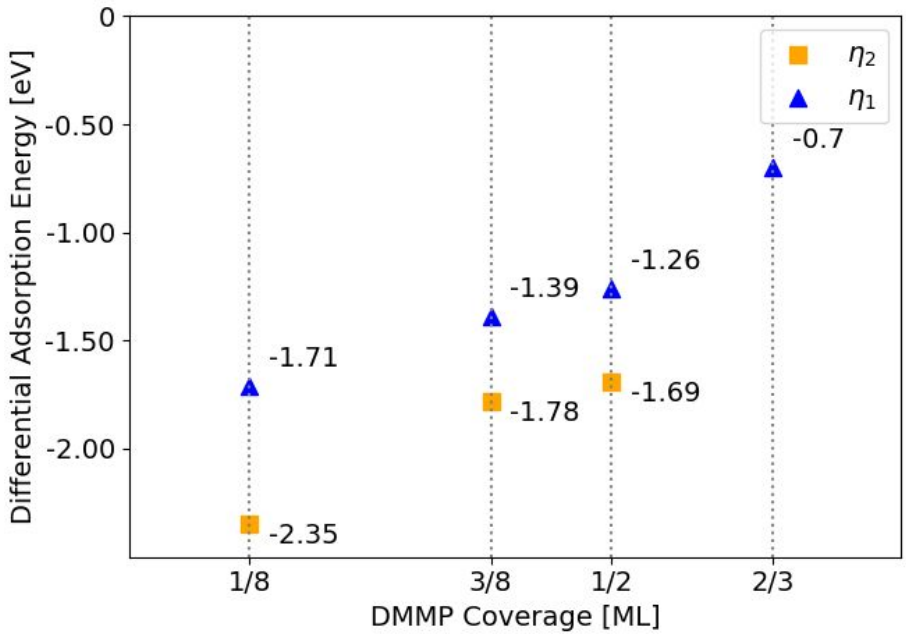

Figure 5: Influence of DMMP coverage on the differential adsorption energy (eV) on r-TiO_2(110). Coverage explored: 1/8, 1/3, 1/2, and 2/3 ML. (ML corresponds to the number of DMMP adsorbed per available Ti_{5c} sites; 1/8ML = 1DMMP/8Ti_{5c} sites).

The decomposition reactivity has been studied at low molecular coverage. Indeed, experiment show that the initial process is DMMP desorption until a lower coverage is reached and reactivity can occur at high temperature. Upon molecular adsorption of DMMP, three different decomposition pathways can be initiated: (1) cleavage of a P-OCH_3 bond, resulting in the adsorption of a methoxy (O_DCH_3, the D subscript meaning that the O atom is coming from DMMP) on a surface Ti_{5c}, (2) cleavage of a O-CH_3 bond, resulting in the adsorption of a methyl group on surface O_{2c} and therefore formation of a O_sCH_3 unit, the s subscript meaning that the O atom comes from the surface, or (3) cleavage of the P-C_I bond, forming also a O_sCH_3 unit. Our calculations show that the P-C_I bond cleavage is not favored thermodynamically on TiO_2, so that reaction pathways were not explored. Thermodynamic analysis of pathways following P-C_I bond cleavage is

featured in the supporting information (page 11 and fig. S9). The C-H bond cleavage pathway was not studied since there is no experimental evidence for this reaction.[26]

Figure 6 shows the energy profile for the DMMP decomposition on the pristine r-TiO_2(110) surface initiated by the cleavage of the P-O_{II} bond. Starting from the most stable adsorption mode of DMMP (structure S1, Fig.4), the cleavage of the P-O_{II} bond yields an intermediate S2 that is thermodynamically downhill by 0.37 eV (36 kJ/mol). However, the path towards breaking this bond has a very high barrier. The activation barrier for the cleavage of the P-O_{II} bond (path S1-S2) is 2.18 eV (210 kJ/mol). The transition state involves breaking of the P-O_{II} bond and creation of the O_{2c}-P bond on the opposite side of the P atom, completing the methoxy transfer onto Ti_{5c} through a 5 coordinated trigonal bi-pyramid like P environment (see SI figure S10 for distances). The structure of the rutile surface and the adsorption mode of DMMP are such that P is initially far from the O_{2c} atom (3.77 Å). The pathway is hence rather long, involving a strong rearrangement of the molecule, and as a result the barrier is high, since the P-O_{II} bond breaking and O_{2c}-P bond formation cannot be completely simultaneously, but rather more sequentially.

Following the initial P-O_{II} bond cleavage (fig. 6, S2), intermediate S2 may opt to cleave the O_{III}-C_{III} yielding intermediate S2a or cleave the P-O_{II} bond, yielding intermediate S2b. The breaking of an O_{III}-C_{III} bond of S2 transfers a methyl onto a surface bridging O_{2c}. Despite yielding a more stable intermediate (S2a) by 0.71 eV (69 kJ/mol) in comparison to the P-O_{III} bond cleavage (S2b), the barrier to breaking the O_{III}-C_{III} bond is high: 2.21 eV (213 kJ/mol) from S2.

The alternative, breaking the P-O_{III} bond is thermodynamically uphill by 0.97 eV (94 kJ/mol), transferring another methoxy onto a surface Ti_{5c}. This step yields an intermediate where the P center is interacting with a surface O_{3c} (fig. 6, S3) to maintain tetrahedral coordination for the organophosphorus, keeping the system stable. The energy barrier to break the P-O_{III} bond in a second step (1.44 eV, 139 kJ/mol) is still high, but lower than that of the first step (P-O_{II}).

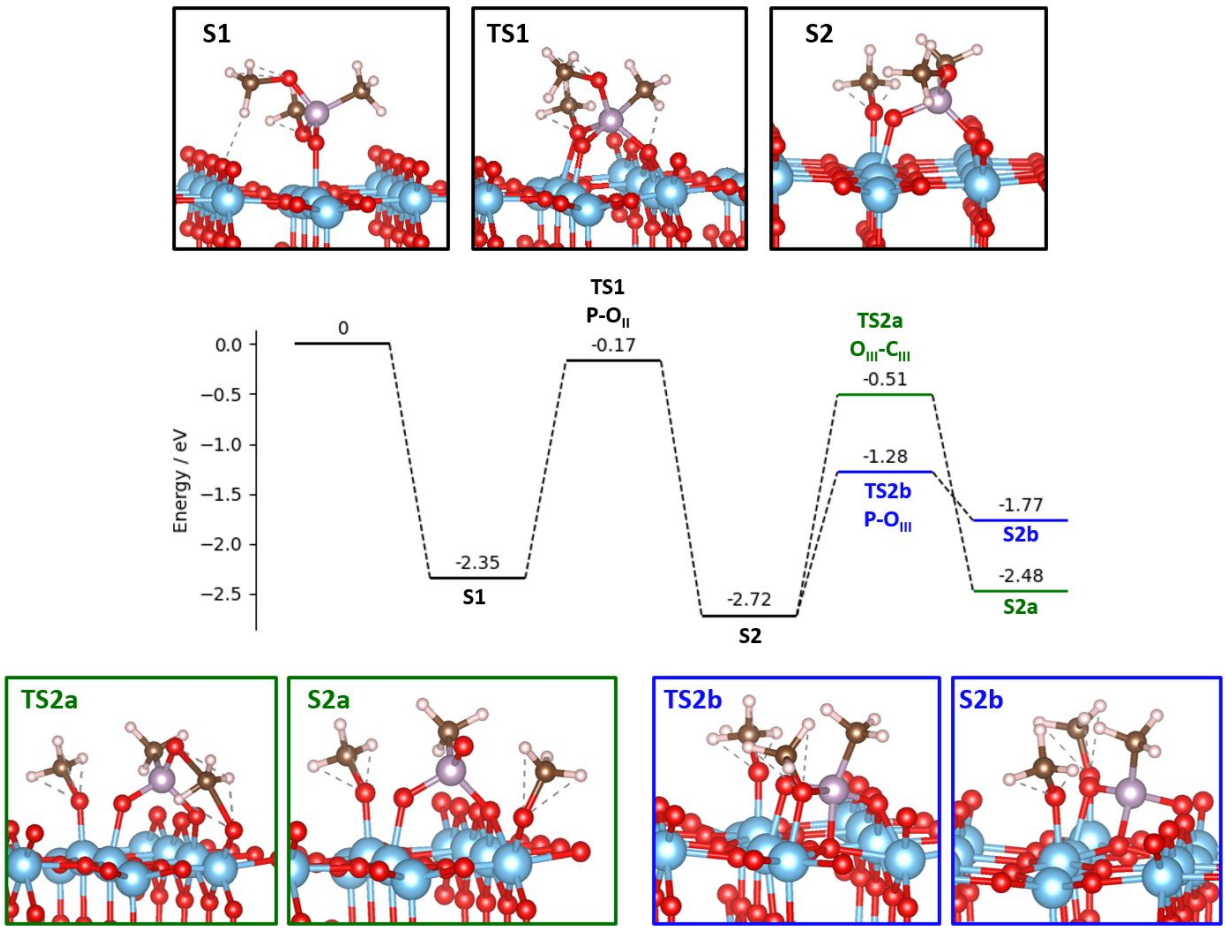

Figure 6: Electronic energy diagram of the decomposition pathway of DMMP initiated via P-OCH_3 bond cleavage on pristine r-TiO_2(110).

Table S3 shows the predicted kinetic rate constant at 300K and 600K for each decomposition step of DMMP on a pristine surface. A quick glance shows that the reaction would not likely proceed on the pristine surface even at elevated temperatures. This is

not surprising as the first step to initiate full decomposition has a high energy barrier to break the initial P-OCH_3 bond. Therefore, decomposition starting from P-OCH_3 bond cleavage is unlikely on the pristine r-TiO_2(110) surface.

The decomposition pathway initiated via the O-CH_3 bond cleavage for DMMP on the pristine surface is depicted in figure 7, with intermediates showcased in the green boxes representing the pathway initiated with O_{II}-C_{II} cleavage and intermediates in the red boxes representing the pathway initiated with O_{III}-C_{III} cleavage.

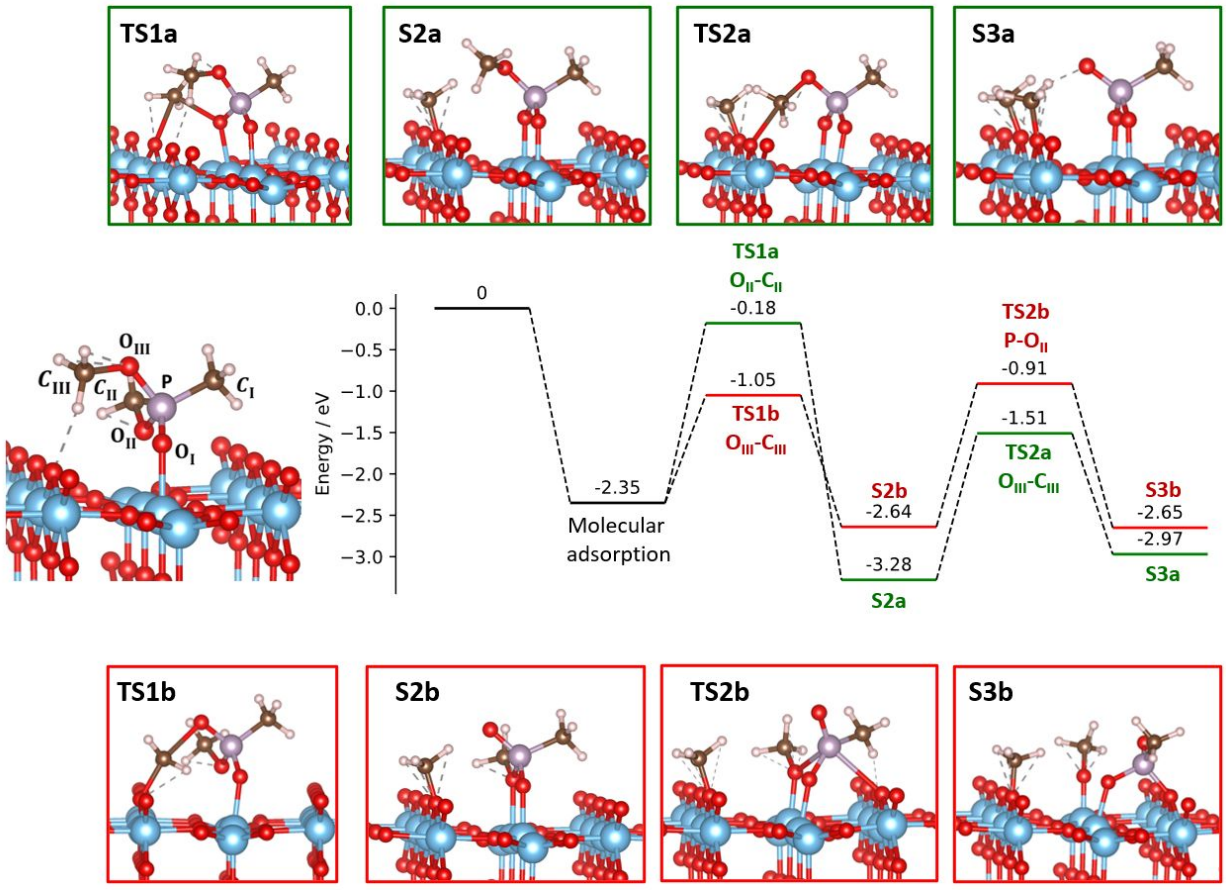

Figure 7: Reaction pathway for DMMP decomposition on the pristine TiO_2 (110) surface via O_{II}-C_{II} and O_{III}-C_{III} bond cleavage. Intermediates of decomposition initiated with O_{II}-C_{II} cleavage are shown in green boxes (path a), whereas intermediates of decomposition initiated with O_{III}-C_{III} cleavage are shown in red boxes (path b).

Following the pathway initiated with O_{II}-C_{II} bond cleavage (Figure 7, path a, green), the activation barrier for initial O_{II}-C_{II} bond breaking is high at 2.17 eV (209 kJ/mol, TS1a). This high barrier indicates that the breaking of the O_{II}-C_{II} bond is highly unlikely at room temperature due to the molecular distortion required to get C_{II} close to a surface O_{2c}. This O_{II}-C_{II} cleavage is nevertheless yielding an intermediate S2a which is more stable by 0.93 eV (89 kJ/mol) compared to the initial adsorption state. This stability of the intermediate after O_{II}-C_{II} cleavage is explained by the fact that P retains its preferred tetragonal coordination, including two O-Ti_{5c} bonds, but again the path to reach this stable intermediate is very unlikely. Further decomposition possibilities beyond the S2a intermediate include breaking the O_{III}-C_{III} bond as it is already well-positioned above a surface O_{2c}. O_{III}-C_{III} cleavage occurs via an SN_2-like attack of O_{2c} on C_{III}, with inversion of configuration. This step nevertheless requires overcoming a barrier of 1.78 eV (172 kJ/mol, TS2a). After the cleavage of O_{II}-C_{II} and O_{III}-C_{III} bonds, the phosphorus-containing product remains in the phosphonate form and is more stable by 0.62 eV compared to molecularly adsorbed DMMP. This decomposition pathway initiated by O_{II}-C_{II} is however associated with high barriers.

The alternate pathway initiated with the O_{III}-C_{III} bond cleavage is described as path b in figure 7 (in red). As explained before in the second step of path a, the O_{III}-C_{III} bond itself is already close to a surface O_{2c}, which is ideal for SN_2-like attack by O_{2c}, with inversion of configuration at the carbon. The direct O_{III}-C_{III} bond cleavage as a first step yields intermediate S2b, which includes an O_sCH_3 species (s denotes surface oxygen) and is more stable by 0.29 eV than molecular adsorption. The barrier for this step is only 1.2 eV (115 kJ/mol, TS1b), much smaller than that of the previously described O_{II}-C_{II} cleavage,

due to the much more favorable position of the CH_3 group with respect to the bridging O_{2c}. Following the transfer of methyl to the surface, a second C-O cleavage (O_{II}-C_{II}) is not favorable (as seen before), but the remaining P fragment has an option to break the P-O_{II} bond, transferring a methoxy group on a surface Ti_{5c} atom and forming intermediate S2b including a O_DCH_3 fragment. The transition state (TS2b) for this step requires sideways rotation of $O=P(O)CH_3$ to ensure that the P center retains its tetrahedral coordination. The energy barrier for this step is however still high at 1.73 eV, so that this reaction is slow even at 600K. The remaining organophosphate product on the surface (S3b) shows similar stability in comparison to intermediate S2b.

Tables S4 and S5 show the calculated rate constant for DMMP decomposition initiated by O_{II}-C_{II} and O_{III}-C_{III} bond cleavages at 300 K and 600 K. The table shows that decomposition via the C-O bond is kinetically possible at high temperatures (600K) and that it would initiate via O_{III}-C_{III} cleavage, not O_{II}-C_{II}. It also shows that the rate constant at 600 K for the second step of P-O cleavage forming O_DCH3 is low (0.04 s-1)).

Further surface methoxy reactivity on the pristine r-TiO_2(110) surface

The pathways of DMMP decomposition on the pristine TiO_2 surface can produce at around 600K surface methyl groups (O_SCH_3) and with much lower rate methoxy groups (O_DCH_3). We consider here the further transformation of these species to check if gas phase molecules can be produced. We include O_DCH_3 to be exhaustive, although its rate constant of formation is low at 600K. The formation and desorption of methanol and formaldehyde from two O_s-CH_3 species are highly endothermic (see Fig S11 in the SI) since it would require the formation of two O vacancies and is hence not possible at all.

The reaction between O_SCH_3 and O_DCH_3 is also unfavorable (Fig S12). One possible reactivity is the formation of formaldehyde from the dehydrogenation of O_DCH_3. The energy profile is shown in figure 8. The formation of formaldehyde is endothermic by 0.54 eV on the surface, and by at least 1.64 eV in the gas phase. This path would hence require very high temperature: at 600K the desorption is still endergonic by 0.17 eV.

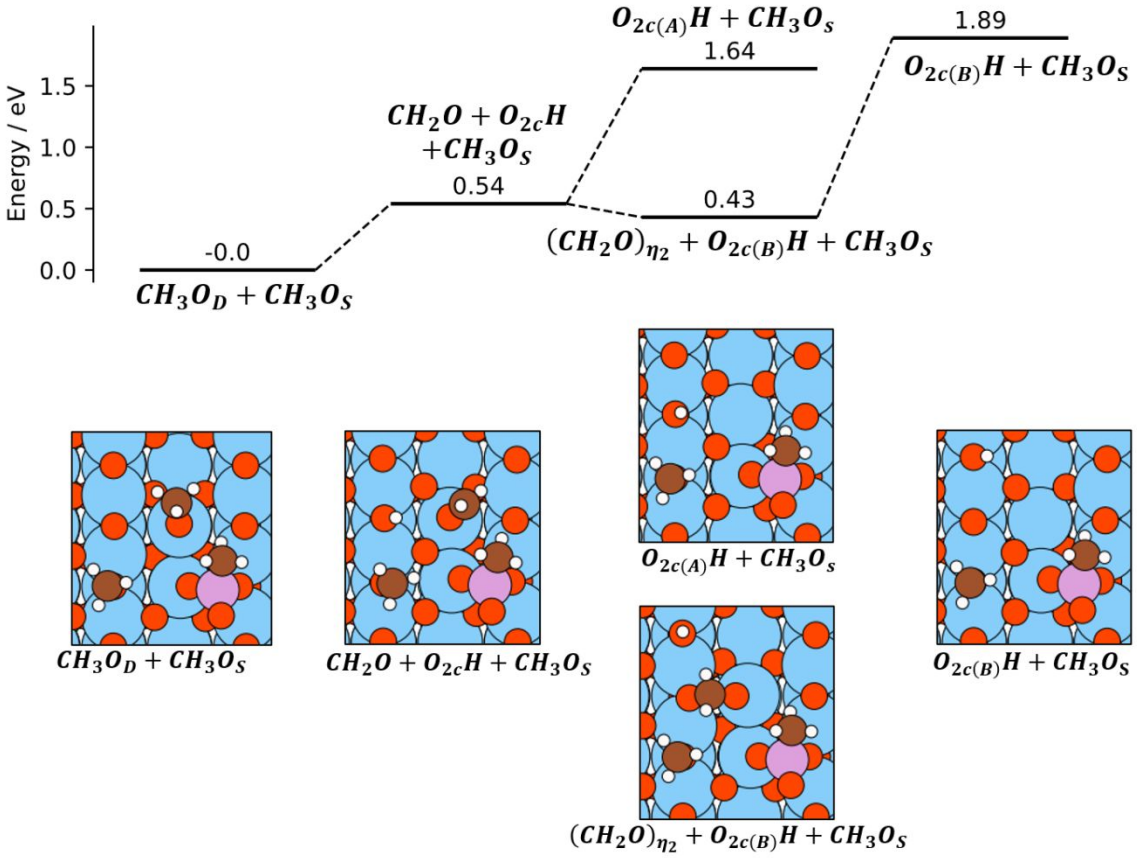

Figure 8: Reaction pathway for the disproportionation reaction between O_sCH_3 and O_DCH_3 resulting from DMMP decomposition on the pristine TiO_2(110) surface.

Surface diffusion could promote reactivity between otherwise separated fragments. We probed the diffusion of O_DCH_3 and H on the r-TiO_2(110) surface. Diffusion of these species along the rows of the (110) surface is easy at reaction temperature (~600K) (with barriers of 0.99 and ~0.8 eV, respectively), however diffusion in the direction

perpendicular to the rows is difficult (for example the diffusion of H from O_{2c} to O_{3c} produces an intermediate that is thermodynamically uphill by 1.1 eV). Hence isotropic diffusion is not possible on the surface and as a result the reaction between two O_DCH_3 produced by the decomposition of distinct DMMP molecules is improbable. Surface O_DCH_3 fragments need to be formed in close proximity to efficiently react. This might not be the case for the pristine surface where each DMMP can give only one surface O_DCH_3.

DMMP adsorption and decomposition on r-TiO_2(110) with O vacancy

The most stable molecular adsorption of DMMP on the TiO_2 (110) surface with a surface bridging vacancy occurs via an interaction between the oxo O_I of DMMP and the oxygen vacancy, with additional interaction of oxygen of DMMP methoxy group (O_{II}) and neighboring Ti_{5c} (fig. 9). This configuration is similar to the configuration on the pristine TiO_2 surface, except that now O_I is occupying the defect site instead of interacting with a surface Ti_{5c}. This conformation yields an adsorption energy of -2.29 eV (221 kJ/mol). The O_I to Ti_{6c} (resp. O_{II} to surface Ti_{5c}) distance is 2.11 Å (resp. 2.42 Å).

Though the P=O group prefers to occupy the vacancy, the presence of the oxygen vacancy counterintuitively slightly decreases the adsorption energy (by 0.06 eV) compared to the pristine surface. This is because the formation of the oxygen vacancy leaves two electrons on the surface Ti_{5c} atoms, therefore reducing the Lewis acidity of titania, and slightly weakening the O_{II}-Ti_{5c} interaction. However, structure-wise, DMMP is now able to interact more with the surface in the sense that the P atom is closer to the surface O_{2c} oxygen, which should facilitate the cleavage of either the P-O_{II} or the O_{III}-C_{III} bond in DMMP while preserving the P tetrahedral coordination.

Our aim here is to understand the local impact of the O vacancy on DMMP adsorption, so only low coverage adsorption was considered, assuming that similar high coverage adsorption would occur on the defective surface, compared to the pristine one. Similar to the case on the pristine surface, we will investigate DMMP decomposition via 3 channels, P-OCH_3, O-CH_3 and P-CH_3 bond cleavage. Again, the P-CH_3 cleavage is not favored thermodynamically (see supporting information page 16 and fig S13).

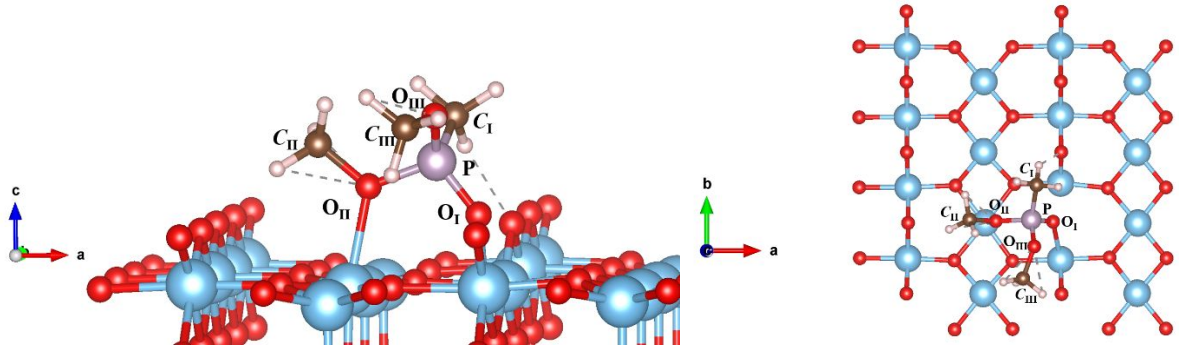

Figure 9: Side (left) and top (right) views of the most stable molecular DMMP adsorption form on r-TiO_2(110) with an oxygen vacancy. O_I occupies the oxygen vacancy with an extra interaction of a DMMP methoxy group (O_{II}) with surface Ti_{5c}.

Starting from the adsorbed state (fig. 9), DMMP decomposition may be initiated via P-O_{II} bond cleavage, forming a methoxy group on a surface Ti_{5c} and a methyl methylphosphonate (MMP) fragment whilst adding a new bond between P and surface O_{2c}. Figure 10 shows these DMMP decomposition pathways on the surface with O vacancy.

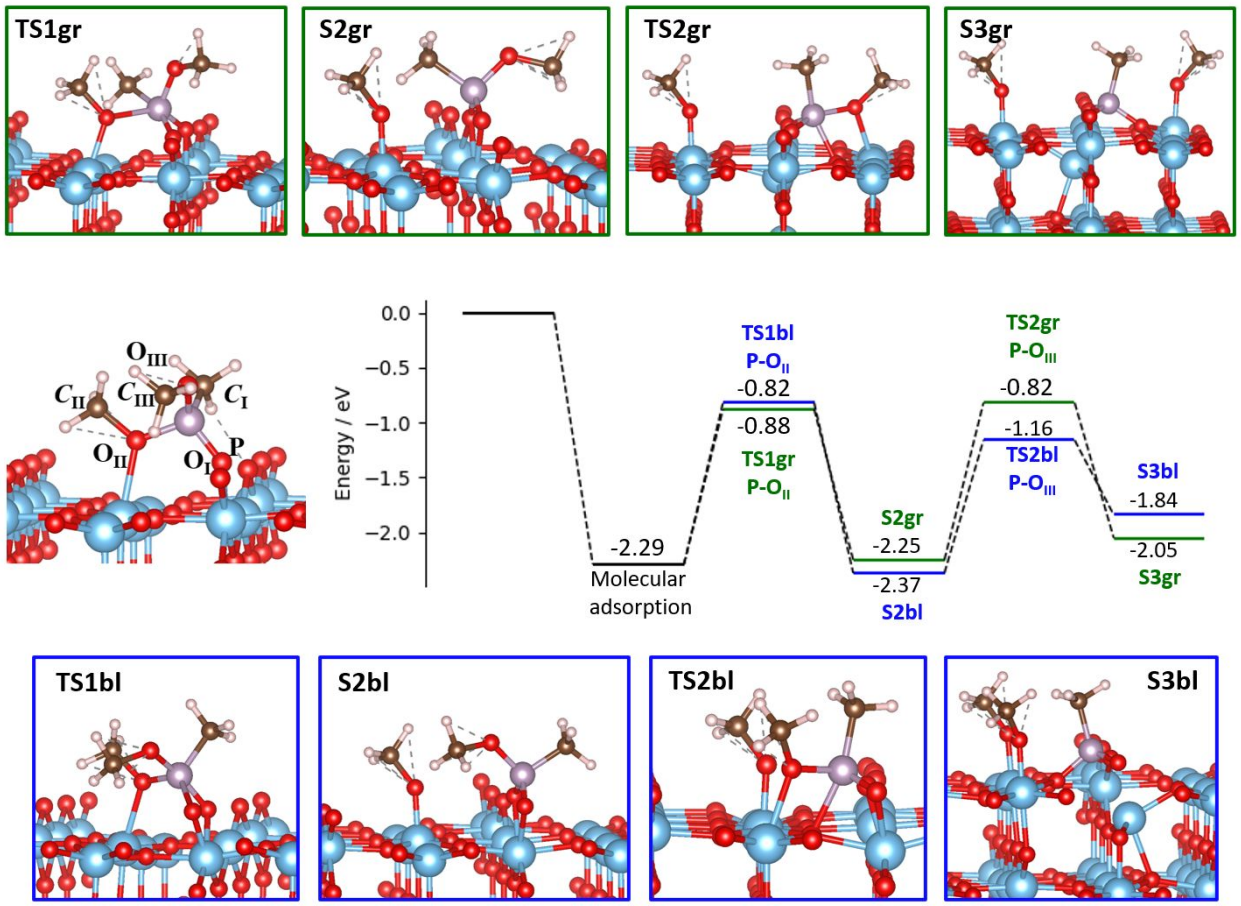

Figure 10: DMMP decomposition initiated via P-O_{II} bond cleavage on r-TiO_2(110) with one O vacancy. Intermediates in green and blue depict decomposition following two possible isomers resulting from P-O_{II} bond cleavage.

There are two possible isomers for the intermediate after P-O_{II} bond cleavage (fig. 11), corresponding to the two ways in which P could interact with O_{2c} after P-OCH_3 bond cleavage. In both cases, the barrier to cleave the P-OCH_3 bond on the defective surface is significantly lower than that on the pristine surface, mainly for a geometric reason. P is geometrically closer to the surface O_{2c} which helps stabilize it by coordinating with the surface upon P-OCH_3 bond cleavage.

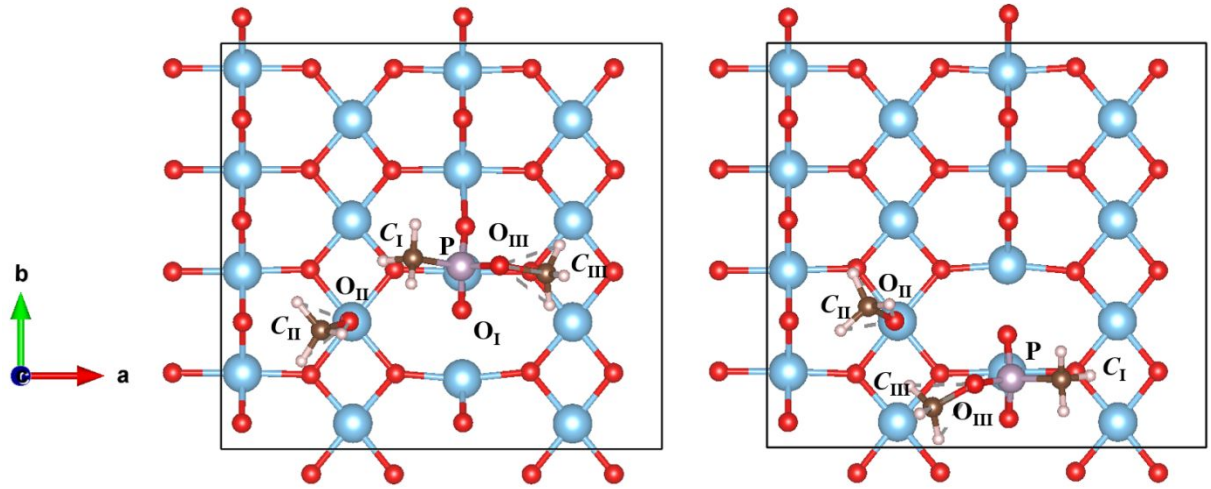

Figure 11: Intermediate isomers upon P-O_{II} bond cleavage on defective TiO_2(110). (left) the remaining CH_3O substituent on P (O_{III}-C_{III}) is pointing away from the adsorbed methoxy resulting from cleavage (S2gr in figure 10, energy: -2.25 eV); (right) the remaining CH_3O on P (O_{III}-C_{III}) is pointing towards the adsorbed methoxy resulting from cleavage. (S2bl in figure 10, energy: -2.37 eV).

The first isomer (fig. 11, left) corresponds to the case where the methoxy substituent of the remaining methyl methylphosphonate (MMP) (O_{III}-C_{III}) is pointing away from the cleaved methoxy group, and it will start the *'green pathway'*. The second isomer (fig. 11, right) has a methoxy substituent of MMP (O_{III}-C_{III}) on the same side as the adsorbed methoxy (O_{II}-C_{II}). The pathway following this second intermediate will be denoted as the *'blue pathway'*. Both isomers have similar adsorption energy as can be expected, -2.25 eV and -2.37 eV for S2 on green and blue pathways, respectively (Fig. 10). This indicates that the P-OCH_3 bond cleavage yields intermediates with similar stability as the molecularly adsorbed DMMP (E = -2.29 eV). The barrier to cleaving the first P-OCH_3 bond is 1.47 eV and 1.41 eV for the green and blue pathways respectively, which is smaller by around 0.77 eV compared to the case of the pristine surface. The transition state for each isomer (TS1bl or TS1gr) involves P interacting with bridging O_{2c} rows prior to the P-OCH_3 bond cleavage (SI fig S14).

The second decomposition step can happen via the breaking of the second P-OCH_3 bond from the remaining MMP intermediates (S2gr or S2bl). Due to the difference in the methoxy group position between the two MMP intermediate isomers, subsequent breaking of the P-OCH_3 bond leads to the formation of the second methoxy on different Ti_{5c} rows (fig. S15). Both cases are slightly endothermic. Following the green pathway, subsequent breaking of the P-O_{III} bond forms an intermediate (S3gr in fig. 10 and fig. S15) which is less stable by 0.24 eV (23 kJ/mol) with respect to the molecularly adsorbed DMMP. P clearly tries to conserve its tetrahedral coordination as it creates a new bond with surface O_{3c} upon P-O_{III} bond cleavage. This configuration forces Ti_{6c} underneath P to shift downwards by 0.64 Å. The barrier to breaking the P-O_{III} is moderate (1.43 eV).

On the blue pathway, after the second P-OCH_3 bond cleavage (P-O_{III}), both methoxy groups are adsorbed on the same Ti_{5c} row (fig. S15 right). This intermediate (S3bl) is however high in energy, less stable than its equivalent isomer in the green pathway by 0.21 eV, and by 0.45 eV (43 kJ/mol) with respect to the molecularly adsorbed DMMP. This is likely due to the proximity of the two adsorbed methoxy groups. The barrier to breaking P-O_{III} bond through this isomer is however slightly lower (1.21 eV, 117 kJ/mole).

Overall, the energy barriers that are required to be passed remain significant (1.4-1.5 eV) so that at room temperature, the kinetic rate constant for every decomposition step is extremely small, like those on a pristine surface. However, the decomposition becomes possible at around 600 K (rate constant ~10 s^{-1}) and the decomposition rate is 6 orders of magnitude faster than that on the pristine surface (tables S6 and S7).

Figure 12 depicts the reaction pathway initiated via O-CH_3 bond cleavage of DMMP on the defective surface. Upon adsorption, there are again two possible O-CH_3 bonds to cleave, O_{II}-C_{II} which interacts with surface $Ti_{5c,}$ and the O_{III}-C_{III} bond which weakly interacts with bridging O_{2c} row via van der Waals interactions.

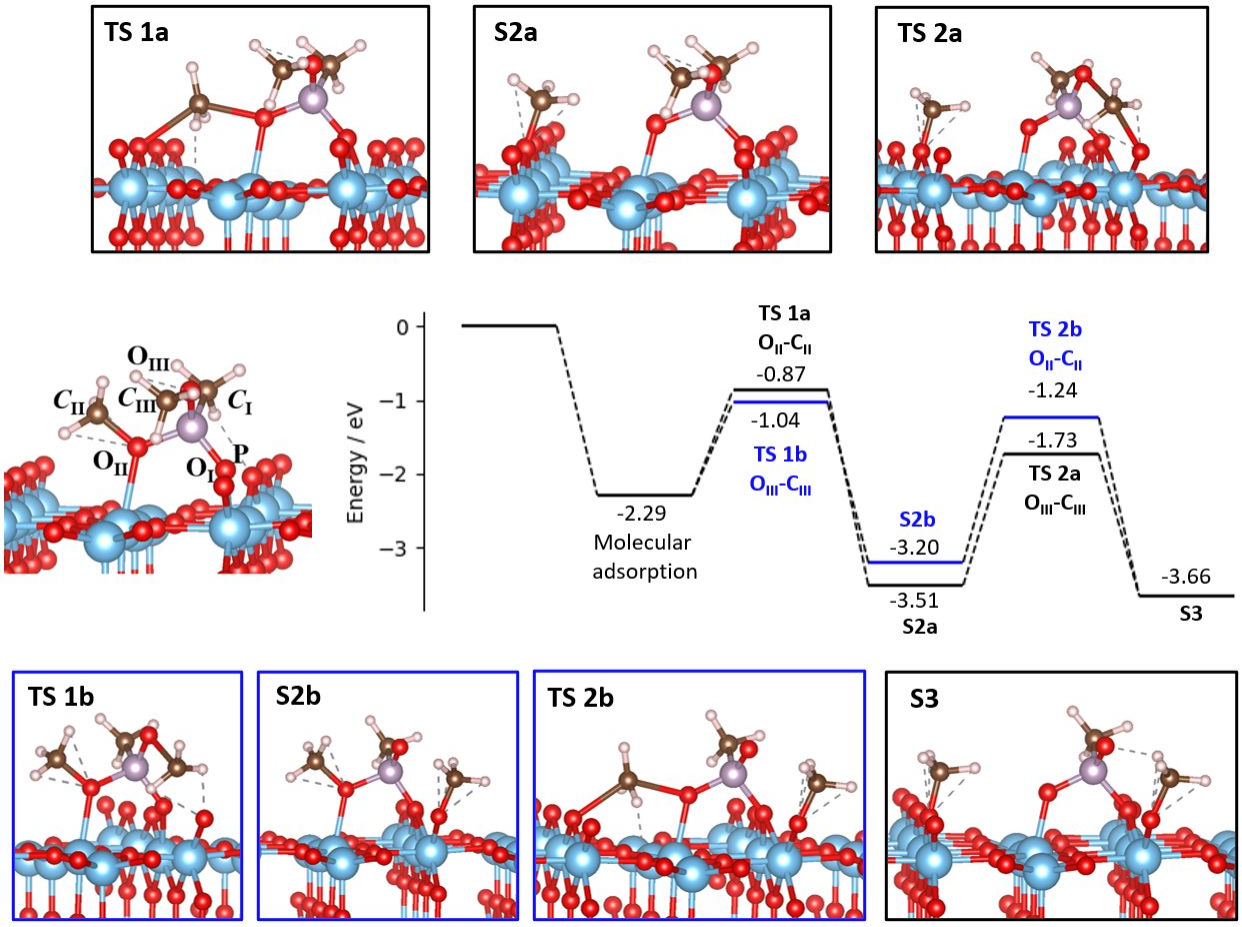

Figure 12: DMMP decomposition initiated via O-C bond cleavage on r-TiO_2(110) with one O vacancy. Intermediates in black (resp. in blue) correspond to decomposition starting from O_{II}-C_{II} bond cleavage, path a (resp. O_{III}-C_{III} bond cleavage, path b).

The path initiated via the O_{II}-C_{II} bond cleavage (denoted as the black path (a) in figure 12), is exothermic and yields a stable intermediate (S2a, -3.51 eV), just as it was shown already in the case on the pristine surface, leaving a methyl on the opposite bridging oxygen row of the remaining P fragment. This intermediate is 1.22 eV more stable than

the adsorption state. The barrier to cleave this bond through TS1a is 1.42 eV, which is much smaller than the barrier for O_{II}-C_{II} cleavage on the pristine surface (2.17 eV). In the case of the O vacancy surface, DMMP is rotated by 90° around the vertical axis, since the P=O group interacts with the vacancy instead of the Ti5c, and this provides a much better initial position to cleave the O_{II}-C_{II} bond. A second decomposition step could follow with the O_{III}-C_{III} bond cleavage, yielding S3 but the barrier is high (1.78 eV).

The path initiated via O_{III}-C_{III} bond cleavage (denoted as the blue path b in figure 12), yields also a stable intermediate (S2b), 0.91 eV more stable than chemisorbed DMMP, leaving a methyl on the same bridging oxygen row, beside the remaining $P(OTi)_2(CH_3)(OCH_3)$ surface species. The barrier to cleave this bond is 1.25 eV, which is very similar to the value for the same O_{III}-C_{III} cleavage on the pristine r-TiO_2(110) (1.20 eV, Fig. 7). A second decomposition step can follow with the O_{II}-C_{II} bond cleavage. The formed intermediate (S3) is 0.46 eV more stable than S2b but the barrier to cleave this O_{II}-C_{II} bond is rather high, 1.96 eV. Altogether, the easiest C-O cleavage reactivity is not significantly modified on the TiO_2 surface with O vacancy, being still the O_{III}-C_{III} dissociation with a very similar barrier compared to the pristine surface.

For both the blue and the black pathways of figure 12, we investigated the P-OCH_3 bond cleavage as a potential second step after the first O-C cleavage, but this was found to be unfavorable (See SI figure S16).

The minimum barrier for decomposition via O-C bond cleavage on the defective surface is hence mostly unchanged by the presence of the O vacancy. It would hence only occur at high temperature (~600 K), where the first dissociation step either via O_{II}-C_{II} or O_{III}-C_{III}

bond cleavage (TS1a and TS1b) proceeds considerably fast, but further decomposition remains difficult (SI tables S8 and S9).

Further surface methoxy reactivity on the r-TiO2(110) surface with O vacancy

We will start from the intermediate species after two P-O bond cleavages (S3bl from fig. 10) that contain two neighboring O_DCH_3, a configuration hence favorable for the formation of formaldehyde and methoxy. The energy diagram is shown in figure 13, while the free energy profile at 600K and the overall thermodynamics as a function of temperature are provided in SI Figure S17 and S18, respectively. The C-H bond cleavage on one O_DCH_3 group occurs with a barrier of 1.20 eV (116 kJ.mol^{-1}) producing η_1 formaldehyde and O_sH. The transfer of H reduces the Ti_{5c} site which hosts the formaldehyde. The O_s-H and H-CH_2O distances are 1.20 Å and 1.40 Å respectively. The diffusion of the proton along the row enables the transformation to η_2 formaldehyde, a process that is stabilizing by 0.93 eV with a barrier of 0.8 eV. The formation of η_2 formaldehyde has previously been experimentally seen in the literature.[118,126,127] The proton can then be transferred to the second methoxy group forming methanol with a very low barrier (0.26 eV). Desorption of formaldehyde and methanol can then proceed, but with significantly positive desorption energies so that the process would only happen at a temperature of ~600 K (desorption is calculated to be favorable in free energy by 0.37 eV at 600 K). An alternative pathway consists in desorbing the η_1 formaldehyde as soon as it is formed, which is endothermic by 0.93 eV then combines the remaining proton on the surface with methoxy to form methanol than can desorb.

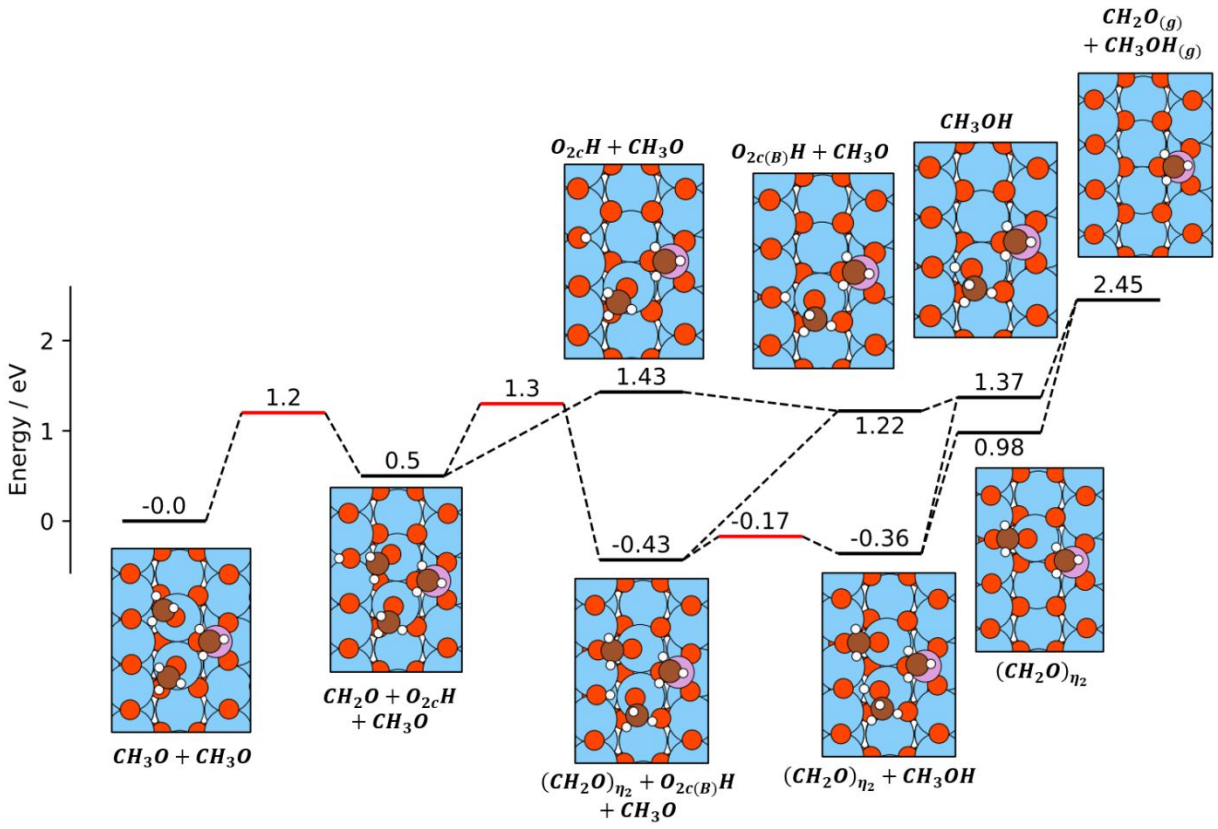

Figure 13 Reaction pathway for methoxy disproportionation reaction forming formaldehyde and methanol between 2 O_sCH_3 resulting from DMMP decomposition on the TiO_2(110) surface with one O vacancy.

The key point of that reactivity study of surface methoxy groups is that the barriers are moderate (effective barrier ~1.3 eV) hence lower than that for DMMP decomposition. Formaldehyde and methanol desorption will then occur as soon as neighboring O_DCH_3 fragments are formed by consecutive P-O cleavage.

Discussion

Our experiments and calculations concur on a high coverage of DMMP at low temperatures. Upon temperature increase the first process is desorption of the weakest bound DMMP, first molecules with only van der Waals and electrostatic interactions

(Eads~0.7 eV) around 300K, then η_1 bound molecules (Eads ~1.1-1.4 eV) around 400-500 K. At higher temperature desorption of η_2 molecules starts to proceed, in competition with their decomposition initiated around 600 K.

The decomposition reactivity pathways of DMMP in r-TiO_2(110) strongly depend on the presence of O vacancies. On pristine r-TiO_2(110), our DFT calculations show that decomposition by P-CH_3 bond cleavage is thermodynamically unfavorable, while P-OCH_3 cleavage leads to stable intermediates, but shows a very high barrier (2.18 eV or 210 kJ/mol) and is therefore kinetically very slow. The only reasonable reactivity would be the cleavage of one of the O-CH_3 bonds, with a barrier of 1.2 eV (116 kJ/mol) which can be passed at ~600K, transferring a methyl group on the bridging oxygen row and forming an O_s-CH_3 fragment. It is interesting to note that the transfer of the methyl group from DMMP to the O atom on the surface occurs with the inversion of the configuration at the carbon. However, the formation and desorption of methanol and formaldehyde from two O_s-CH_3 species, requiring the formation of two O vacancies, is highly endothermic. Further decomposition from the product of O-C bond cleavage could occur through P-O bond cleavage, with a barrier of 1.73 eV, still corresponding to a low rate at 600 K. We showed however that further reactivity of the eventually produced single O_DCH_3 fragment is thermodynamically difficult and that diffusion that could bring two methoxy species together is very slow perpendicular to the rows of the substrate. This suggests that the decomposition of DMMP on the pristine TiO_2 surface, by C-O bond and then P-O bond cleavage, although possible at a high temperature cannot easily provide gas-phase products.

The r-TiO_2(110) surface with an O vacancy is markedly more reactive for P-O bond cleavage, generating a methoxy group O_DCH_3 and MMP, with a barrier of 1.4 eV, reduced by 0.7 eV compared to pristine r-TiO_2. Further decomposition by the second P-O cleavage shows similar barriers. Upon P-O bond cleavage, the formed MMP fragments require to be stabilized by an additional interaction between P and a titania surface O, to compensate for the broken P-O bond. On the pristine surface, this additional P-O interaction cannot be formed easily because DMMP is chemisorbed with the P atom relatively high on the surface, so the reaction requires an important re-orientation of the molecule. The presence of the O vacancy enables a chemisorption mode of DMMP closer to the surface, hence making the rebinding of the P atom more facile, and hence stabilizing the transition state. In the presence of an O vacancy, P-O cleavage on DMMP becomes possible at a temperature of ~ 600 K (SI table S6-S7). The formed neighboring surface methoxy species can desorb as methanol and formaldehyde by disproportionation. The transformation of two O_DCH_3 surface species in gas phase methanol and formaldehyde is proceeding with barriers that are lower than that of the decomposition of DMMP and is calculated to be thermodynamically favorable by 0.37 eV at 600 K. This contrast with the case of the pristine surface where desorption of formaldehyde is endergonic by 0.17 eV at that same temperature.

We then conclude that DMMP molecules chemisorbed in the vicinity of an O vacancy can undergo at ~600 K two P-OCH3 bond cleavages, yielding two neighboring methoxy groups that can evolve into formaldehyde and methanol gas-phase product. In contrast, DMMP molecules chemisorbed far from O vacancy can undergo one C-O and, with lower rate, one P-O bond cleavage but can less favorably produce gas-phase products. Results

from calculations are in good agreement with our TPD experiment, where the amount of formaldehyde and methanol products is similar to that of the number of O vacancies on the surface. This combination of experiment and calculations shows that O vacancies are the main active site for the high temperature decomposition of DMMP by double P-O bond cleavage, yielding formaldehyde and methanol.

Previous surface science experiments in the literature on the decomposition of DMMP on r-TiO_2(110) saw different products (methane and H_2).[26] As we have shown here, the reactivity of that surface is strongly dependent on the presence of O vacancies. We hypothesize that the r-TiO_2(110) surface in the previous experiments had a high level of reduction with a high coverage of O vacancies. Surface methoxy species can produce methyl and methane on highly reduced TiO_2 samples.[118,128] Our experiments are performed with less than 2% of a monolayer of O vacancies so that we did not detect any other products than formaldehyde and methanol.

The single-crystal surface used here shows distinct reactivity compared to high surface area powder TiO_2 samples. As presented in the introduction, powder TiO_2 shows a higher reactivity towards DMMP, with P-O cleavage around room temperature. We showed here that defects in TiO_2 are very important for the DMMP decomposition reactivity, and powder TiO_2 presents a large number of defects, notably surface OH groups which are not present in our highly dehydrated single crystal surface. These hydroxyl groups have been proposed as active sites for DMMP reactivity on powder TiO_2.[19,25,30] Additionally, DMMP decomposition on other metal oxides such as Al_2O_3 and MOF suggests that surface hydroxyl promotes the P-OCH_3 bond dissociation.[6,34,35,129]

Several calculated pathways involving the O-CH_3 bond and P-OCH_3 cleavages on the pristine and partially reduced r-TiO_2(110) show high barriers but produce surface species after decomposition which are more stable than DMMP. This indicates that if the bond cleavage steps are accelerated by a catalyst, the decomposition products of DMMP can be efficiently stabilized on r-TiO_2 surfaces. This suggests that TiO_2 is a good candidate to serve as efficient support for dispersed metal catalysts (nanoparticles or single atoms) for DMMP oxidative decomposition, in the sense that P containing products could migrate and be stabilized on the TiO_2, hence freeing the main catalytic site (nanoparticles) for further reaction.

Conclusion

In this work, we have performed DFT calculations and TPD experiments on thermal DMMP decomposition on both pristine and defective surfaces of TiO_2(110). Molecular adsorption on a pristine surface happens via the interaction of the oxo (P=O) oxygen with surface Ti_{5c} centers, with an additional interaction from one methoxy group with a neighboring Ti_{5c}. On the defective surface, DMMP adsorbs with the oxo (P=O) oxygen occupying the vacancy site, still completed by binding of a methoxy group on Ti_{5c}. A strong dependence of DMMP adsorption energy on coverage is found in our calculations, from weakly bound molecules (Eads=-0.7 eV), to covalently bound η_1 molecule (Eads= -1.2 to -1.7 eV), to strongly bound η_2 configurations (Eads=-1.7 to -2.35 eV). The reactivity of the TiO_2(110) surface is shown to be overall low, with mainly molecular desorption and only a small fraction of methanol and formaldehyde decomposition products seen from TPD

at around 650K. In addition, the amount of products is similar to the number of O vacancies on the surface.

Our calculations explore the possibility to decompose chemisorbed DMMP by P-O, C-O, and P-C bond cleavage. P-C bond breaking is found to lead to thermodynamically unstable decomposition products. P-OCH_3 bond dissociation is thermodynamically possible but kinetically hindered on the pristine r-TiO_2(110) surface. Oxygen vacancy on r-TiO_2 is essential to reduce the energy barrier for P-OCH_3 breaking and make that reaction kinetically possible at around 600 K. For stability reasons, the cleaved P-O bond in DMMP must be replaced by the formation of a new P-O bond with surface oxygen. The geometry of DMMP on the pristine r-TiO_2 surface is such that these reactive elementary steps cannot be concerted, and thus the barrier is high. In the presence of an oxygen vacancy, DMMP lies closer to the surface, reducing the barrier by ~0.7 eV. The formed surface methoxy groups (O_DCH_3) can desorb as methanol and formaldehyde at ~600 K, in good agreement with our TPD experiments. DFT also shows that O-C bond cleavage of DMMP is a viable pathway at high temperature (600K) for DMMP decomposition on the pristine surface and the surface with O vacancies. This first C-O cleavage can be followed by P-O dissociation on the pristine TiO_2 surface. However, that decomposition channel can less favorably yield gas-phase products, making the O vacancy-assisted double P-O bond cleavage the main channel for formaldehyde and methanol production at around 600 K on r-TiO_2(110).

Our study also reveals that, upon decomposition, P-containing residues stay on the surface even after heating up to 750 K, indicating that r-TiO_2(110) is a good support to trap the DMMP decomposition products. The strong adsorption of DMMP and excellent

stability of intermediates upon decomposition make TiO_2 a support of choice for DMMP oxidation catalysts since it enables the storage of the reaction products.

Conflicts of interest

There are no conflicts of interest to declare.

Acknowledgments

We gratefully acknowledge the support of this work by the US army under Program No W911NF2020183 and W911NF-21-1-0361. This work used the Extreme Science and Engineering Discovery Environment (XSEDE), which is supported by the National Science Foundation grant number ACI-1548562. This work used computational and storage services associated with the Hoffman2 Shared Cluster provided by UCLA Institute for Digital Research and Education's Research Technology Group.

References

(1) Sanderson, H. Chemical Warfare Agents. In *Encyclopedia of Environmental Health*; Elsevier, 2011; pp 587–596. https://doi.org/10.1016/B978-0-444-52272-6.00386-X.

(2) King, A. M.; Aaron, C. K. Organophosphate and Carbamate Poisoning. *Emergency Medicine Clinics of North America*. 2015. https://doi.org/10.1016/j.emc.2014.09.010.

(3) Gupta, R. C. *Handbook of Toxicology of Chemical Warfare Agents*; Elsevier, 2015. https://doi.org/10.1016/C2013-0-15402-5.

(4) Trotochaud, L.; Tsyshevsky, R.; Holdren, S.; Fears, K.; Head, A. R.; Yu, Y.;

Karslıoğlu, O.; Pletincx, S.; Eichhorn, B.; Owrutsky, J.; Long, J.; Zachariah, M.; Kuklja, M. M.; Bluhm, H. Spectroscopic and Computational Investigation of Room-Temperature Decomposition of a Chemical Warfare Agent Simulant on Polycrystalline Cupric Oxide. *Chem. Mater.* **2017**, *29* (17), 7483–7496. https://doi.org/10.1021/acs.chemmater.7b02489.

(5) Head, A. R.; Trotochaud, L.; Tsyshevsky, R.; Fears, K.; Eichhorn, B.; Kuklja, M. M.; Bluhm, H. Coupling Ambient Pressure X-Ray Photoelectron Spectroscopy with Density Functional Theory to Study Complex Surface Chemistry and Catalysis. *Top. Catal.* **2018**. https://doi.org/10.1007/s11244-018-1062-7.

(6) Head, A. R.; Tsyshevsky, R.; Trotochaud, L.; Yu, Y.; Kyhl, L.; Karslıoğlu, O.; Kuklja, M. M.; Bluhm, H. Adsorption of Dimethyl Methylphosphonate on MoO 3 : The Role of Oxygen Vacancies. *J. Phys. Chem. C* **2016**, *120* (51), 29077–29088. https://doi.org/10.1021/acs.jpcc.6b07340.

(7) Head, A. R.; Tsyshevsky, R.; Trotochaud, L.; Yu, Y.; Karslıoğlu, O.; Eichhorn, B.; Kuklja, M. M.; Bluhm, H. Dimethyl Methylphosphonate Adsorption and Decomposition on MoO2 as Studied by Ambient Pressure X-Ray Photoelectron Spectroscopy and DFT Calculations. *J. Phys. Condens. Matter* **2018**, *30* (13), 134005. https://doi.org/10.1088/1361-648X/aab192.

(8) Segal, S. R.; Cao, L.; Suib, S. L.; Tang, X.; Satyapal, S. Thermal Decomposition of Dimethyl Methylphosphonate over Manganese Oxide Catalysts. *J. Catal.* **2001**, *198* (1), 66–76. https://doi.org/10.1006/jcat.2000.3126.

(9) Mitchell, M. B.; Sheinker, V. N.; Tesfamichael, A. B.; Gatimu, E. N.; Nunley, M.

Decomposition of Dimethyl Methylphosphonate (DMMP) on Supported Cerium and Iron Co-Impregnated Oxides at Room Temperature. *J. Phys. Chem. B* **2003**. https://doi.org/10.1021/jp021836m.

(10) Bermudez, V. M. Quantum-Chemical Study of the Adsorption of DMMP and Sarin on γ-Al 2 O 3. *J. Phys. Chem. C* **2007**, *111* (9), 3719–3728. https://doi.org/10.1021/jp066439g.

(11) Sheinker, V. N.; Mitchell, M. B. Quantitative Study of the Decomposition of Dimethyl Methylphosphonate (DMMP) on Metal Oxides at Room Temperature and Above. *Chem. Mater.* **2002**. https://doi.org/10.1021/cm010758x.

(12) Li, Y. X.; Koper, O.; Atteya, M.; Klabunde, K. J. Adsorption and Decomposition of Organophosphorus Compounds on Nanoscale Metal Oxide Particles. In Situ GC-MS Studies of Pulsed Microreactions over Magnesium Oxide. *Chem. Mater.* **1992**. https://doi.org/10.1021/cm00020a019.

(13) Li, Y. X.; Klabunde, K. J. Nanoscale Metal Oxide Particles as Chemical Reagents. Destructive Adsorption of a Chemical Agent Simulant, Dimethyl Methylphosphonate, on Heat-Treated Magnesium Oxide. *Langmuir* **1991**. https://doi.org/10.1021/la00055a017.

(14) Wagner, G. W.; Bartram, P. W.; Koper, O.; Klabunde, K. J. Reactions of VX, GD, and HD with Nanosize MgO. *J. Phys. Chem. B* **1999**. https://doi.org/10.1021/jp984689u.

(15) Sharma, N.; Kakkar, R. Adsorption of Sarin on MgO Nanotubes: Role of Doped and Defect Sites. *J. Comput. Sci.* **2015**.

https://doi.org/10.1016/j.jocs.2014.12.003.

(16) Chen, D. A.; Ratliff, J. S.; Hu, X.; Gordon, W. O.; Senanayake, S. D.; Mullins, D. R. Dimethyl Methylphosphonate Decomposition on Fully Oxidized and Partially Reduced Ceria Thin Films. *Surf. Sci.* **2010**, *604* (5–6), 574–587. https://doi.org/10.1016/j.susc.2009.12.028.

(17) Henderson, M. A.; Jin, T.; White, J. M. A TPD/AES Study of the Interaction of Dimethyl Methylphosphonate with Iron Oxide (.Alpha.-Fe2O3) and Silicon Dioxide. *J. Phys. Chem.* **1986**, *90* (19), 4607–4611. https://doi.org/10.1021/j100410a027.

(18) Walenta, C. A.; Xu, F.; Tesvara, C.; O'Connor, C. R.; Sautet, P.; Friend, C. M. Facile Decomposition of Organophosphonates by Dual Lewis Sites on a Fe3O4(111) Film. *J. Phys. Chem. C* **2020**. https://doi.org/10.1021/acs.jpcc.0c01708.

(19) Trubitsyn, D. A.; Vorontsov, A. V. Experimental Study of Dimethyl Methylphosphonate Decomposition over Anatase TiO 2. *J. Phys. Chem. B* **2005**, *109* (46), 21884–21892. https://doi.org/10.1021/jp053793q.

(20) Rusu, C. N.; Yates, J. T. Adsorption and Decomposition of Dimethyl Methylphosphonate on TiO 2. *J. Phys. Chem. B* **2000**, *104* (51), 12292–12298. https://doi.org/10.1021/jp002560q.

(21) Panayotov, D. A.; Morris, J. R. Thermal Decomposition of a Chemical Warfare Agent Simulant (DMMP) on TiO2: Adsorbate Reactions with Lattice Oxygen as Studied by Infrared Spectroscopy. *J. Phys. Chem. C* **2009**.

https://doi.org/10.1021/jp9036233.

(22) Panayotov, D. A.; Morris, J. R. Catalytic Degradation of a Chemical Warfare Agent Simulant: Reaction Mechanisms on TiO2-Supported Au Nanoparticles. *J. Phys. Chem. C* **2008**. https://doi.org/10.1021/jp7118668.

(23) Kim, K.; Tsay, O. G.; Atwood, D. A.; Churchill, D. G. Destruction and Detection of Chemical Warfare Agents. *Chemical Reviews*. 2011. https://doi.org/10.1021/cr100193y.

(24) Mitchell, M. B.; Sheinker, V. N.; Mintz, E. A. Adsorption and Decomposition of Dimethyl Methylphosphonate on Metal Oxides. *J. Phys. Chem. B* **1997**. https://doi.org/10.1021/jp972724b.

(25) Panayotov, D. A.; Morris, J. R. Thermal Decomposition of a Chemical Warfare Agent Simulant (DMMP) on TiO 2 : Adsorbate Reactions with Lattice Oxygen as Studied by Infrared Spectroscopy. *J. Phys. Chem. C* **2009**, *113* (35), 15684–15691. https://doi.org/10.1021/jp9036233.

(26) Zhou, J.; Varazo, K.; Reddic, J. .; Myrick, M. .; Chen, D. A. Decomposition of Dimethyl Methylphosphonate on TiO2(110): Principal Component Analysis Applied to X-Ray Photoelectron Spectroscopy. *Anal. Chim. Acta* **2003**, *496* (1–2), 289–300. https://doi.org/10.1016/S0003-2670(03)01008-0.

(27) Head, A. R.; Tang, X.; Hicks, Z.; Wang, L.; Bleuel, H.; Holdren, S.; Trotochaud, L.; Yu, Y.; Kyhl, L.; Karslıoğlu, O.; Fears, K.; Owrutsky, J.; Zachariah, M.; Bowen, K. H.; Bluhm, H. Thermal Desorption of Dimethyl Methylphosphonate from MoO3. *Catal. Struct. React.* **2017**. https://doi.org/10.1080/2055074X.2017.1278891.

(28) Ratliff, J. S.; Tenney, S. A.; Hu, X.; Conner, S. F.; Ma, S.; Chen, D. A. Decomposition of Dimethyl Methylphosphonate on Pt, Au, and Au-Pt Clusters Supported on TiO 2 (110). *Langmuir* **2009**. https://doi.org/10.1021/la802361q.

(29) Tang, X.; Hicks, Z.; Wang, L.; Ganteför, G.; Bowen, K. H.; Tsyshevsky, R.; Sun, J.; Kuklja, M. M. Adsorption and Decomposition of Dimethyl Methylphosphonate on Size-Selected (MoO 3) 3 Clusters. *Phys. Chem. Chem. Phys.* **2018**, *20* (7), 4840–4850. https://doi.org/10.1039/C7CP08427G.

(30) Panayotov, D. A.; Morris, J. R. Uptake of a Chemical Warfare Agent Simulant (DMMP) on TiO 2 : Reactive Adsorption and Active Site Poisoning. *Langmuir* **2009**, *25* (6), 3652–3658. https://doi.org/10.1021/la804018b.

(31) Kim, C. S.; Lad, R. J.; Tripp, C. P. Interaction of Organophosphorous Compounds with TiO2 and WO3 Surfaces Probed by Vibrational Spectroscopy. *Sensors Actuators B Chem.* **2001**, *76* (1–3), 442–448. https://doi.org/10.1016/S0925-4005(01)00653-0.

(32) Templeton, M. K.; Weinberg, W. H. Adsorption and Decomposition of Dimethyl Methylphosphonate on an Aluminum Oxide Surface. *J. Am. Chem. Soc.* **1985**. https://doi.org/10.1021/ja00287a018.

(33) Pehrsson, P.; Gordon, W.; Balow, R.; Barlow, D.; Bermudez, V. M.; Iordanov, I.; Knox, C.; Lundin, J.; Wynne, J. H.; Karwacki, C. J.; Peterson, G. W. DMMP Reactivity on Zirconium Hydroxide under in Operando Conditions. In *Abstracts of Papers, 251st ACS National Meeting & Exposition, San Diego, CA, United States, March 13-17, 2016*; 2016.

(34) Wang, G.; Sharp, C.; Plonka, A. M.; Wang, Q.; Frenkel, A. I.; Guo, W.; Hill, C.; Smith, C.; Kollar, J.; Troya, D.; Morris, J. R. Mechanism and Kinetics for Reaction of the Chemical Warfare Agent Simulant, DMMP(g), with Zirconium(IV) MOFs: An Ultrahigh-Vacuum and DFT Study. *J. Phys. Chem. C* **2017**. https://doi.org/10.1021/acs.jpcc.7b00070.

(35) Ruffley, J. P.; Goodenough, I.; Luo, T. Y.; Richard, M.; Borguet, E.; Rosi, N. L.; Johnson, J. K. Design, Synthesis, and Characterization of Metal-Organic Frameworks for Enhanced Sorption of Chemical Warfare Agent Simulants. *J. Phys. Chem. C* **2019**. https://doi.org/10.1021/acs.jpcc.9b05574.

(36) Plonka, A. M.; Wang, Q.; Gordon, W. O.; Balboa, A.; Troya, D.; Guo, W.; Sharp, C. H.; Senanayake, S. D.; Morris, J. R.; Hill, C. L.; Frenkel, A. I. In Situ Probes of Capture and Decomposition of Chemical Warfare Agent Simulants by Zr-Based Metal Organic Frameworks. *J. Am. Chem. Soc.* **2017**, *139* (2), 599–602. https://doi.org/10.1021/jacs.6b11373.

(37) Henderson, M. A.; Otero-Tapia, S.; Castro, M. E. The Chemistry of Methanol on the TiO2(110) Surface: The Influence of Vacancies and Coadsorbed Species. *Faraday Discuss.* **1999**. https://doi.org/10.1039/a902070e.

(38) de Armas, R. S.; Oviedo, J.; San Miguel, M. A.; Sanz, J. F. Methanol Adsorption and Dissociation on TiO 2 (110) from First Principles Calculations. *J. Phys. Chem. C* **2007**, *111* (27), 10023–10028. https://doi.org/10.1021/jp0717701.

(39) Wang, F.; Wei, S.; Zhang, Z.; Patzke, G. R.; Zhou, Y. Oxygen Vacancies as Active Sites for H2S Dissociation on the Rutile TiO2(110) Surface: A First-

Principles Study. *Phys. Chem. Chem. Phys.* **2016**. https://doi.org/10.1039/c5cp06835e.

(40) Schaub, R.; Thostrup, P.; Lopez, N.; Lægsgaard, E.; Stensgaard, I.; Nørskov, J. K.; Besenbacher, F. Oxygen Vacancies as Active Sites for Water Dissociation on Rutile TiO2(110). *Phys. Rev. Lett.* **2001**. https://doi.org/10.1103/PhysRevLett.87.266104.

(41) Cai, Q.; Wang, F.; He, J.; Dan, M.; Cao, Y.; Yu, S.; Zhou, Y. Oxygen Defect Boosted Photocatalytic Hydrogen Evolution from Hydrogen Sulfide over Active {0 0 1} Facet in Anatase TiO2. *Appl. Surf. Sci.* **2020**. https://doi.org/10.1016/j.apsusc.2020.146198.

(42) Diebold, U. Structure and Properties of TiO2 Surfaces: A Brief Review. *Appl. Phys. A Mater. Sci. Process.* **2003**. https://doi.org/10.1007/s00339-002-2004-5.

(43) Dulub, O.; Valentin, C. Di; Selloni, A.; Diebold, U. Structure, Defects, and Impurities at the Rutile TiO2(0 1 1)-(2 × 1) Surface: A Scanning Tunneling Microscopy Study. *Surf. Sci.* **2006**. https://doi.org/10.1016/j.susc.2006.06.042.

(44) Ganduglia-Pirovano, M. V.; Hofmann, A.; Sauer, J. Oxygen Vacancies in Transition Metal and Rare Earth Oxides: Current State of Understanding and Remaining Challenges. *Surface Science Reports*. 2007. https://doi.org/10.1016/j.surfrep.2007.03.002.

(45) Pan, X.; Yang, M.-Q.; Fu, X.; Zhang, N.; Xu, Y.-J. Defective TiO2 with Oxygen Vacancies: Synthesis, Properties and Photocatalytic Applications. *Nanoscale* **2013**, *5* (9), 3601. https://doi.org/10.1039/c3nr00476g.

(46) Wei, H.; Liu, X.; Wang, A.; Zhang, L.; Qiao, B.; Yang, X.; Huang, Y.; Miao, S.; Liu, J.; Zhang, T. FeOx-Supported Platinum Single-Atom and Pseudo-Single-Atom Catalysts for Chemoselective Hydrogenation of Functionalized Nitroarenes. *Nat. Commun.* **2014**, *5* (1), 5634. https://doi.org/10.1038/ncomms6634.

(47) Di Valentin, C.; Pacchioni, G.; Selloni, A. Electronic Structure of Defect States in Hydroxylated and Reduced Rutile TiO2(110) Surfaces. *Phys. Rev. Lett.* **2006**. https://doi.org/10.1103/PhysRevLett.97.166803.

(48) Morgan, B. J.; Watson, G. W. A DFT + U Description of Oxygen Vacancies at the TiO2 Rutile (1 1 0) Surface. *Surf. Sci.* **2007**. https://doi.org/10.1016/j.susc.2007.08.025.

(49) Li, H.; Guo, Y.; Robertson, J. Calculation of TiO2 Surface and Subsurface Oxygen Vacancy by the Screened Exchange Functional. *J. Phys. Chem. C* **2015**. https://doi.org/10.1021/acs.jpcc.5b02430.

(50) Cheng, H.; Selloni, A. Surface and Subsurface Oxygen Vacancies in Anatase TiO2 and Differences with Rutile . *Phys. Rev. B* **2009**. https://doi.org/10.1103/physrevb.79.092101.

(51) Gong, X. Q.; Khorshidi, N.; Stierle, A.; Vonk, V.; Ellinger, C.; Dosch, H.; Cheng, H.; Selloni, A.; He, Y.; Dulub, O.; Diebold, U. The 2 × 1 Reconstruction of the Rutile TiO2(0 1 1) Surface: A Combined Density Functional Theory, X-Ray Diffraction, and Scanning Tunneling Microscopy Study. *Surf. Sci.* **2009**. https://doi.org/10.1016/j.susc.2008.10.034.

(52) Göpel, W.; Rocker, G.; Feierabend, R. Intrinsic Defects of TiO2(110): Interaction

with Chemisorbed O2, H2, CO, and CO2. *Phys. Rev. B* **1983**. https://doi.org/10.1103/PhysRevB.28.3427.

(53) Pan, J. -M.; Maschhoff, B. L.; Diebold, U.; Madey, T. E. Interaction of Water, Oxygen, and Hydrogen with TiO 2 (110) Surfaces Having Different Defect Densities . *J. Vac. Sci. Technol. A Vacuum, Surfaces, Film.* **1992**. https://doi.org/10.1116/1.577986.

(54) Yu, Y. Y.; Gong, X. Q. CO Oxidation at Rutile TiO2(110): Role of Oxygen Vacancies and Titanium Interstitials. *ACS Catal.* **2015**. https://doi.org/10.1021/cs501900q.

(55) Kim, H. Y.; Lee, H. M.; Pala, R. G. S.; Shapovalov, V.; Metiu, H. CO Oxidation by Rutile TiO2(110) Doped with V, W, Cr, Mo, and Mn. *J. Phys. Chem. C* **2008**. https://doi.org/10.1021/jp802296g.

(56) Petrik, N. G.; Kimmel, G. A. Off-Normal CO2 Desorption from the Photooxidation of CO on Reduced TiO2(110). *J. Phys. Chem. Lett.* **2010**. https://doi.org/10.1021/jz100884w.

(57) Wang, L.; Shultz, A. N.; Baer, D. R.; Engelhard, M. H. Interactions of Small Molecules with TiO 2 (110) Surfaces: The Role of Defects . *J. Vac. Sci. Technol. A Vacuum, Surfaces, Film.* **1996**. https://doi.org/10.1116/1.580291.

(58) Henrich, V. E.; Dresselhaus, G.; Zeiger, H. J. Chemisorbed Phases of H2O on TiO2 and SrTiO3. *Solid State Commun.* **1977**. https://doi.org/10.1016/0038-1098(77)90376-3.

(59) Brookes, I. M.; Muryn, C. A.; Thornton, G. Imaging Water Dissociation on TiO2(110). *Phys. Rev. Lett.* **2001**. https://doi.org/10.1103/PhysRevLett.87.266103.

(60) Zhang, Z.; Bondarchuk, O.; Kay, B. D.; White, J. M.; Dohnálek, Z. Imaging Water Dissociation on TiO2(110): Evidence for Inequivalent Geminate OH Groups. *J. Phys. Chem. B* **2006**. https://doi.org/10.1021/jp063619h.

(61) Petrik, N. G.; Kimmel, G. A. Reaction Kinetics of Water Molecules with Oxygen Vacancies on Rutile TiO2(110). *J. Phys. Chem. C* **2015**. https://doi.org/10.1021/acs.jpcc.5b07526.

(62) Shen, M.; Henderson, M. A. Site Competition during Coadsorption of Acetone with Methanol and Water on TiO2(110). *Langmuir* **2011**. https://doi.org/10.1021/la2016726.

(63) Henderson, M. A. Structural Sensitivity in the Dissociation of Water on TiO2 Single-Crystal Surfaces. *Langmuir* **1996**. https://doi.org/10.1021/la960360t.

(64) Henderson, M. A. The Interaction of Water with Solid Surfaces: Fundamental Aspects Revisited. *Surface Science Reports*. 2002. https://doi.org/10.1016/s0167-5729(01)00020-6.

(65) Eriksen, S.; Naylor, P. D.; Egdell, R. G. The Adsorption of Water on SrTiO3 and TiO2: A Reappraisal. *Spectrochim. Acta - Part A Mol. Spectrosc.* **1987**. https://doi.org/10.1016/S0584-8539(87)80043-0.

(66) Brinkley, D.; Dietrich, M.; Engel, T.; Farrall, P.; Gantner, G.; Schafer, A.;

Szuchmacher, A. A Modulated Molecular Beam Study of the Extent of H2O Dissociation on TiO2(110). *Surf. Sci.* **1998**. https://doi.org/10.1016/S0039-6028(97)00633-X.

(67) Hugenschmidt, M. B.; Gamble, L.; Campbell, C. T. The Interaction of H2O with a TiO2(110) Surface. *Surf. Sci.* **1994**. https://doi.org/10.1016/0039-6028(94)90837-0.

(68) Bermudez, V. M. Effect of Humidity on the Interaction of Dimethyl Methylphosphonate (DMMP) Vapor with SiO2 and Al2O3 Surfaces, Studied Using Infrared Attenuated Total Reflection Spectroscopy. *Langmuir* **2010**. https://doi.org/10.1021/la103381r.

(69) Kurtz, R. L.; Stock-Bauer, R.; Msdey, T. E.; Román, E.; De Segovia, J. L. Synchrotron Radiation Studies of H2O Adsorption on TiO2(110). *Surf. Sci.* **1989**. https://doi.org/10.1016/0039-6028(89)90626-2.

(70) Bullock, E. L.; Patthey, L.; Steinemann, S. G. Clean and Hydroxylated Rutile TiO2(110) Surfaces Studied by X-Ray Photoelectron Spectroscopy. *Surf. Sci.* **1996**. https://doi.org/10.1016/0039-6028(95)01188-9.

(71) Petrik, N. G.; Zhang, Z.; Du, Y.; Dohnálek, Z.; Lyubinetsky, I.; Kimmel, G. A. Chemical Reactivity of Reduced TiO 2(110): The Dominant Role of Surface Defects in Oxygen Chemisorption. *J. Phys. Chem. C* **2009**. https://doi.org/10.1021/jp901989x.

(72) Epling, W. S.; Peden, C. H. F.; Henderson, M. A.; Diebold, U. Evidence for Oxygen Adatoms on TiO2(110) Resulting from O2 Dissociation at Vacancy Sites.

Surf. Sci. **1998**. https://doi.org/10.1016/S0039-6028(98)00446-4.

(73) Henderson, M. A.; Epling, W. S.; Perkins, C. L.; Peden, C. H. F.; Diebold, U. Interaction of Molecular Oxygen with the Vacuum-Annealed TiO2(110) Surface: Molecular and Dissociative Channels. *J. Phys. Chem. B* **1999**. https://doi.org/10.1021/jp990655q.

(74) Kimmel, G. A.; Petrik, N. G. Tetraoxygen on Reduced TiO2(110): Oxygen Adsorption and Reactions with Bridging Oxygen Vacancies. *Phys. Rev. Lett.* **2008**. https://doi.org/10.1103/PhysRevLett.100.196102.

(75) Henderson, M. A.; Otero-Tapia, S.; Castro, M. E. Electron-Induced Decomposition of Methanol on the Vacuum-Annealed Surface of TiO2(110). *Surf. Sci.* **1998**. https://doi.org/10.1016/S0039-6028(98)00434-8.

(76) Zhou, C.; Ma, Z.; Ren, Z.; Mao, X.; Dai, D.; Yang, X. Effect of Defects on Photocatalytic Dissociation of Methanol on TiO 2(110). *Chem. Sci.* **2011**. https://doi.org/10.1039/c1sc00249j.

(77) Zhang, Z.; Bondarchuk, O.; White, J. M.; Kay, B. D.; Dohnálek, Z. Imaging Adsorbate O-H Bond Cleavage: Methanol on TiO2(110). *J. Am. Chem. Soc.* **2006**. https://doi.org/10.1021/ja058466a.

(78) Crampton, A. S.; Cai, L.; Janvelyan, N.; Zheng, X.; Friend, C. M. Methanol Photo-Oxidation on Rutile TiO2 Nanowires: Probing Reaction Pathways on Complex Materials. *J. Phys. Chem. C* **2017**. https://doi.org/10.1021/acs.jpcc.7b01385.

(79) Phillips, K. R.; Jensen, S. C.; Baron, M.; Li, S. C.; Friend, C. M. Sequential Photo-

Oxidation of Methanol to Methyl Formate on TiO 2(110). *J. Am. Chem. Soc.* **2013**. https://doi.org/10.1021/ja3106797.

(80) Jensen, S. C.; Friend, C. M. The Dynamic Roles of Interstitial and Surface Defects on Oxidation and Reduction Reactions on Titania. *Top. Catal.* **2013**. https://doi.org/10.1007/s11244-013-0135-x.

(81) Walenta, C. A.; Tschurl, M.; Heiz, U. Introducing Catalysis in Photocatalysis: What Can Be Understood from Surface Science Studies of Alcohol Photoreforming on TiO2. *Journal of Physics Condensed Matter*. 2019. https://doi.org/10.1088/1361-648X/ab351a.

(82) Walenta, C. A.; Courtois, C.; Kollmannsberger, S. L.; Eder, M.; Tschurl, M.; Heiz, U. Surface Species in Photocatalytic Methanol Reforming on Pt/TiO2(110): Learning from Surface Science Experiments for Catalytically Relevant Conditions. *ACS Catal.* **2020**. https://doi.org/10.1021/acscatal.0c00260.

(83) Walenta, C. A.; Kollmannsberger, S. L.; Courtois, C.; Pereira, R. N.; Stutzmann, M.; Tschurl, M.; Heiz, U. Why Co-Catalyst-Loaded Rutile Facilitates Photocatalytic Hydrogen Evolution. *Phys. Chem. Chem. Phys.* **2019**. https://doi.org/10.1039/c8cp05513k.

(84) Liu, L. M.; Zhao, J. Effects of Oxygen Vacancy on the Adsorption of Formaldehyde on Rutile TiO2(110) Surface. *Chinese J. Chem. Phys.* **2017**. https://doi.org/10.1063/1674-0068/30/cjcp1703049.

(85) Wang, Z.; Xiong, F.; Zhang, Z.; Sun, G.; Xu, H.; Chai, P.; Huang, W. Surface Chemistry of Formaldehyde on Rutile TiO2(011)-(2 × 1) Surface: Photocatalysis

Versus Thermal-Catalysis. *J. Phys. Chem. C* **2017**. https://doi.org/10.1021/acs.jpcc.7b09527.

(86) Haubrich, J.; Kaxiras, E.; Friend, C. M. The Role of Surface and Subsurface Point Defects for Chemical Model Studies on TiO2: A First-Principles Theoretical Study of Formaldehyde Bonding on Rutile TiO2(110). *Chem. - A Eur. J.* **2011**. https://doi.org/10.1002/chem.201002588.

(87) Cremer, T.; Jensen, S. C.; Friend, C. M. Enhanced Photo-Oxidation of Formaldehyde on Highly Reduced o-TiO2(110). *J. Phys. Chem. C* **2014**. https://doi.org/10.1021/jp5053908.

(88) Zhu, K.; Xia, Y.; Tang, M.; Wang, Z. T.; Lyubinetsky, I.; Ge, Q.; Dohnálek, Z.; Park, K. T.; Zhang, Z. Low-Temperature Reductive Coupling of Formaldehyde on Rutile TiO2(110). *J. Phys. Chem. C* **2015**. https://doi.org/10.1021/acs.jpcc.5b05639.

(89) Yuan, Q.; Wu, Z.; Jin, Y.; Xiong, F.; Huang, W. Surface Chemistry of Formaldehyde on Rutile TiO2(110) Surface: Photocatalysis vs Thermal-Catalysis. *J. Phys. Chem. C* **2014**. https://doi.org/10.1021/jp5061733.

(90) Kresse, G.; Furthmüller, J. Efficiency of Ab-Initio Total Energy Calculations for Metals and Semiconductors Using a Plane-Wave Basis Set. *Comput. Mater. Sci.* **1996**. https://doi.org/10.1016/0927-0256(96)00008-0.

(91) Kresse, G.; Furthmüller, J. Software VASP, Vienna. *Phys. Rev. B* **1996**.

(92) Perdew, J. P.; Burke, K.; Ernzerhof, M. Generalized Gradient Approximation

Made Simple. *Phys. Rev. Lett.* **1996**. https://doi.org/10.1103/PhysRevLett.77.3865.

(93) Steinmann, S. N.; Corminboeuf, C. Comprehensive Benchmarking of a Density-Dependent Dispersion Correction. *J. Chem. Theory Comput.* **2011**. https://doi.org/10.1021/ct200602x.

(94) Steinmann, S. N.; Corminboeuf, C. A Generalized-Gradient Approximation Exchange Hole Model for Dispersion Coefficients. *J. Chem. Phys.* **2011**. https://doi.org/10.1063/1.3545985.

(95) Blöchl, P. E. Projector Augmented-Wave Method. *Phys. Rev. B* **1994**. https://doi.org/10.1103/PhysRevB.50.17953.

(96) Kresse, G.; Furthmüller, J. Efficient Iterative Schemes for Ab Initio Total-Energy Calculations Using a Plane-Wave Basis Set. *Phys. Rev. B - Condens. Matter Mater. Phys.* **1996**. https://doi.org/10.1103/PhysRevB.54.11169.

(97) Kresse G.a Joubert, D. . From Ultrasoft Pseudopotentials to the Projector Augmented-Wave Method. *Phys. Rev. B - Condens. Matter Mater. Phys.* **1999**.

(98) Anisimov, V. I.; Aryasetiawan, F.; Lichtenstein, A. I. First-Principles Calculations of the Electronic Structure and Spectra of Strongly Correlated Systems: The LDA + U Method. *Journal of Physics Condensed Matter*. 1997. https://doi.org/10.1088/0953-8984/9/4/002.

(99) Dudarev, S.; Botton, G. Electron-Energy-Loss Spectra and the Structural Stability of Nickel Oxide: An LSDA+U Study. *Phys. Rev. B - Condens. Matter Mater. Phys.*

1998. https://doi.org/10.1103/PhysRevB.57.1505.

(100) Tang, Y.; Asokan, C.; Xu, M.; Graham, G. W.; Pan, X.; Christopher, P.; Li, J.; Sautet, P. Rh Single Atoms on TiO2 Dynamically Respond to Reaction Conditions by Adapting Their Site. *Nat. Commun.* **2019**, *10* (1), 1–18. https://doi.org/10.1038/s41467-019-12461-6.

(101) Deskins, N. A.; Rousseau, R.; Dupuis, M. Distribution of Ti3+ Surface Sites in Reduced TiO2. *J. Phys. Chem. C* **2011**. https://doi.org/10.1021/jp2001139.

(102) Pacchioni, G. Oxygen Vacancy: The Invisible Agent on Oxide Surfaces. *ChemPhysChem*. 2003. https://doi.org/10.1002/cphc.200300835.

(103) Sánchez-Sánchez, C.; González, C.; Jelinek, P.; Méndez, J.; De Andres, P. L.; Martín-Gago, J. A.; López, M. F. Understanding Atomic-Resolved STM Images on TiO2(110)-(1 × 1) Surface by DFT Calculations. *Nanotechnology* **2010**. https://doi.org/10.1088/0957-4484/21/40/405702.

(104) Schaub, R.; Wahlström, E.; Rønnau, A.; Lægsgaard, E.; Stensgaard, I.; Besenbacher, F. Oxygen-Mediated Diffusion of Oxygen Vacancies on the TiO2(110) Surface. *Science (80-.).* **2003**. https://doi.org/10.1126/science.1078962.

(105) Makov, G.; Payne, M. C. Periodic Boundary Conditions in Ab Initio Calculations. *Phys. Rev. B* **1995**. https://doi.org/10.1103/PhysRevB.51.4014.

(106) Ohno, T.; Sarukawa, K.; Tokieda, K.; Matsumura, M. Morphology of a TiO2 Photocatalyst (Degussa, P-25) Consisting of Anatase and Rutile Crystalline

Phases. *J. Catal.* **2001**, *203* (1), 82–86. https://doi.org/10.1006/jcat.2001.3316.

(107) Walenta, C. A.; Crampton, A. S.; Xu, F.; Heiz, U.; Friend, C. M. Chemistry of Methanol and Ethanol on Ozone-Prepared α-Fe2O3(0001). *J. Phys. Chem. C* **2018**. https://doi.org/10.1021/acs.jpcc.8b07574.

(108) Walenta, C. A.; Xu, F.; Tesvara, C.; O'Connor, C. R.; Sautet, P.; Friend, C. M. Facile Decomposition of Organophosphonates by Dual Lewis Sites on a Fe 3 O 4 (111) Film . *J. Phys. Chem. C* **2020**. https://doi.org/10.1021/acs.jpcc.0c01708.

(109) Diebold, U. The Surface Science of Titanium Dioxide. *Surface Science Reports*. 2003. https://doi.org/10.1016/s0167-5729(02)00100-0.

(110) Walenta, C. A.; Kollmannsberger, S. L.; Pereira, R. N.; Tschurl, M.; Stutzmann, M.; Heiz, U. Anhydrous Ethanol Dehydrogenation on Metal-Organic Chemical Vapor Deposition Grown GaN(0001). *J. Phys. Chem. C* **2017**. https://doi.org/10.1021/acs.jpcc.7b04946.

(111) Winstead, C.; McKoy, V. Interaction of Slow Electrons with Methyl Phosphate Esters. *Int. J. Mass Spectrom.* **2008**. https://doi.org/10.1016/j.ijms.2008.04.015.

(112) Bull, J. N.; Harland, P. W.; Vallance, C. Absolute Total Electron Impact Ionization Cross-Sections for Many-Atom Organic and Halocarbon Species. *J. Phys. Chem. A* **2012**. https://doi.org/10.1021/jp210294p.

(113) Harrison, A. G.; Jones, E. G.; Gupta, S. K.; Nagy, G. P. TOTAL CROSS SECTIONS FOR IONIZATION BY ELECTRON IMPACT. *Can. J. Chem.* **1966**. https://doi.org/10.1139/v66-293.

(114) Shen, M.; Henderson, M. A. Identification of the Active Species in Photochemical Hole Scavenging Reactions of Methanol on TiO2. *J. Phys. Chem. Lett.* **2011**. https://doi.org/10.1021/jz201242k.

(115) Courtois, C.; Eder, M.; L. Kollmannsberger, S.; Tschurl, M.; A. Walenta, C.; Heiz, U. Origin of Poisoning in Methanol Photoreforming on TiO2(110): The Importance of Thermal Back-Reaction Steps in Photocatalysis. *ACS Catal.* **2020**, *10* (14), 7747–7752. https://doi.org/10.1021/acscatal.0c01615.

(116) Shen, M.; Henderson, M. A. Role of Water in Methanol Photochemistry on Rutile TiO 2(110). *J. Phys. Chem. C* **2012**. https://doi.org/10.1021/jp3046774.

(117) A. Walenta, C.; Courtois, C.; L. Kollmannsberger, S.; Eder, M.; Tschurl, M.; Heiz, U. Surface Species in Photocatalytic Methanol Reforming on Pt/TiO2(110): Learning from Surface Science Experiments for Catalytically Relevant Conditions. *ACS Catal.* **2020**, *10* (7), 4080–4091. https://doi.org/10.1021/acscatal.0c00260.

(118) Osmić, M.; Mohrhusen, L.; Al-Shamery, K. Bulk Defect Dependence of Low-Temperature Partial Oxidation of Methanol and High-Temperature Hydrocarbon Formation on Rutile TiO2 (110). *J. Phys. Chem. C* **2018**, *123* (13), 7615–7626. https://doi.org/10.1021/acs.jpcc.8b02953.

(119) Ma, S.; Zhou, J.; Kang, Y. C.; Reddic, J. E.; Chen, D. A. Dimethyl Methylphosphonate Decomposition on Cu Surfaces: Supported Cu Nanoclusters and Films on TiO 2(110). *Langmuir* **2004**. https://doi.org/10.1021/la048594x.

(120) Zhou, J.; Ma, S.; Kang, Y. C.; Chen, D. A. Dimethyl Methylphosphonate Decomposition on Titania-Supported Ni Clusters and Films: A Comparison of

Chemical Activity on Different Ni Surfaces. *J. Phys. Chem. B* **2004**. https://doi.org/10.1021/jp040185m.

(121) Yang, L.; Taylor, R.; de Jong, W. A.; Hase, W. L. A Model DMMP/TiO 2 (110) Intermolecular Potential Energy Function Developed from Ab Initio Calculations. *J. Phys. Chem. C* **2011**, *115* (25), 12403–12413. https://doi.org/10.1021/jp1112137.

(122) Yang, L.; Tunega, D.; Xu, L.; Govind, N.; Sun, R.; Taylor, R.; Lischka, H.; DeJong, W. A.; Hase, W. L. Comparison of Cluster, Slab, and Analytic Potential Models for the Dimethyl Methylphosphonate (DMMP)/TiO 2 (110) Intermolecular Interaction. *J. Phys. Chem. C* **2013**, *117* (34), 17613–17622. https://doi.org/10.1021/jp404898v.

(123) Bermudez, V. M. First-Principles Study of Adsorption of Dimethyl Methylphosphonate on the TiO2 Anatase (001) Surface: Formation of a Stable Titanyl (Ti=O) Site. *J. Phys. Chem. C* **2011**. https://doi.org/10.1021/jp200009s.

(124) Bermudez, V. M. Computational Study of the Adsorption of Dimethyl Methylphosphonate (DMMP) on the (0 1 0) Surface of Anatase TiO2 with and without Faceting. *Surf. Sci.* **2010**. https://doi.org/10.1016/j.susc.2010.01.021.

(125) Quintero, Y. C.; Nagarajan, R. Molecular and Dissociative Adsorption of DMMP, Sarin and Soman on Dry and Wet TiO2(110) Using Density Functional Theory. *Surf. Sci.* **2018**. https://doi.org/10.1016/j.susc.2018.04.002.

(126) Mohrhusen, L.; Kräuter, J.; Al-Shamery, K. Conversion of Methanol on Rutile TiO2(110) and Tungsten Oxide Clusters: 2. The Role of Defects and Electron

Transfer in Bifunctional Oxidic Photocatalysts. *Phys. Chem. Chem. Phys.* **2021**, *23* (21). https://doi.org/10.1039/d1cp01176f.

(127) Yu, X.; Zhang, Z.; Yang, C.; Bebensee, F.; Heissler, S.; Nefedov, A.; Tang, M.; Ge, Q.; Chen, L.; D. Kay, B.; Dohnálek, Z.; Wang, Y.; Wöll, C. Interaction of Formaldehyde with the Rutile TiO2(110) Surface: A Combined Experimental and Theoretical Study. *J. Phys. Chem. C* **2016**, *120* (23), 12626–12636. https://doi.org/10.1021/acs.jpcc.6b03689.

(128) Farfan-Arribas, E.; Madix, R. J. Different Binding Sites for Methanol Dehydrogenation and Deoxygenation on Stoichiometric and Defective TiO2(1 1 0) Surfaces. *Surf. Sci.* **2003**, *544* (2–3). https://doi.org/10.1016/j.susc.2003.08.025.

(129) Mitchell, M. B.; Sheinker, V. N.; Mintz, E. A. Adsorption and Decomposition of Dimethyl Methylphosphonate on Metal Oxides. *J. Phys. Chem. B* **1997**, *101* (51), 11192–11203. https://doi.org/10.1021/jp972724b.